THE DIFFUSION OF SOLID PARTICLES IN A TURBULENT GAS STREAM

THE DIFFUSION OF SOLID PARTICLES IN A TURBULENT GAS STREAM

By

LE DINH NAM, B.A.Sc.

A Major Study Report

Submitted to the Faculty of Graduate Studies

in Partial Fulfilment of the Requirements

for the Degree

Master of Engineering

McMaster University

February, 1970

MASTER OF ENGINEERING (1970) McMASTER UNIVERSITY
(Chemical Engineering) Hamilton, Ontario

TITLE: The Diffusion of Solid Particles in a Turbulent Gas Stream

AUTHOR: Le Dinh Nam, B.A.Sc. (Laval University, Quebec)

SUPERVISOR: Professor T.W. Hoffman

NUMBER OF PAGES: xii, 99

SCOPE AND CONTENTS:

An experimental study was performed to measure the diffusion of solid particles in a gas stream flowing turbulently in a 5.5 in. diameter pipe at a Reynolds number of 52800.

Glass beads (density 2.55 g/cm^3) with a size range 0-60 microns and average particle size of 35 microns were injected into the gas stream. The particle motion was observed by measuring the particle concentrations at various radial and axial positions downstream. A solids feeder and a sampling system were designed for this purpose.

A method of analysing the experimental data based on a constant eddy diffusivity of the particles was developed. This analysis indicates that under the conditions studied, the eddy diffusivity of the particles is approximately 60% of that of the gas. The experimental results demonstrate that this model provides a reasonably good approximation to the turbulent diffusion in circular conduits. The results also provide a fairly good picture of the interaction between the fluid and solid particles in turbulent flow.

Some future directions for research in this area are also indicated.

ACKNOWLEDGEMENTS

The author would like to express his appreciation to Dr. T.W. Hoffman, Chairman of the Chemical Engineering Department for his suggestion of the topic and his guidance and advice during the course of this project.

The author is also grateful to Dr. J.H.T. Wade, Chairman of the Mechanical Engineering Department for his kindness in the loan of Koo's apparatus.

Thanks are extended to Mr. J. Newton for his assistance in the design and installation of the equipment.

This project is financially supported by McMaster University and the National Research Council of Canada.

TABLE OF CONTENTS

LIST OF TABLES

LIST OF FIGURES

NOMENCLATURE

a	defined by equation (3-12a)
A, A'	constants in equation (3-16)
A_n	coefficient in nth term of series representing concentration (equation 3-18)
A_p	cross-sectional area of particle, L^2
b	radius of tracer injector tube, L
B, B'	constants in equation (3-16)
C	concentration, number of particles per unit volume of gas
C_i	concentration of particles of size d_i
C_∞	limit of C when $x \to \infty$
$C_{i\infty}$	limit of C_i when $x \to \infty$
$\left(\frac{C}{C_\infty}\right)_n$	normalized relative concentration
C_D	drag coefficient for spheres, dimensionless
C_o	coefficient in equation (A-1)
d	particle diameter, L
d_i	average diameter of particles in size group i, L
d_v	volume average diameter of particles in sample, L
$d_{v\infty}$	volume average diameter of particles in original tracer, L
D	molecular diffusivity, L^2T^{-1}
f	friction factor defined by $u^* = \sqrt{f/8}U$, dimensionless
$f(d_i)$	fraction of particles of size d_i in sample
$f_\infty(d_i)$	fraction of particles of size d_i in original tracer

$f(r)$ function defined by equation (3-8)

F_D drag force, F

g gravitational acceleration, L^2T^{-1}

g_c gravitational constant, $MLF^{-1}T^{-2}$

J_o zero-order Bessel function of the first kind

J_1 first-order Bessel function of the first kind

k defined by equation (7-10a), T^{-1}

K constant in equation (3-14)

ℓ distance from pipe axis in vertical direction that the particle falls, L

m mass of a particle, M

m number of size groups chosen to represent the size distribution

M total mass of particles per unit volume of gas, ML^{-3}

M_i mass of particles of size d_i per unit volume of gas, ML^{-3}

M_∞ limit of M when $x \to \infty$, or W_p/Q, ML^{-3}

n_i number of particles of size d_i

N total mass flux = $N_\ell + N_t$, $MT^{-1}L^{-2}$

N_ℓ laminar mass flux, $MT^{-1}L^{-2}$

N_t turbulent mass flux, $MT^{-1}L^{-2}$

Q volumetric gas flowrate, L^3T^{-1}

r distance from pipe axis, L

R inside radius of pipe, L

Re flow Reynolds number = $2RU\rho/\mu$, dimensionless

Re_p particle Reynolds number = $dv_p\rho/\mu$, dimensionless

S.F.R. abreviation of "Solids Flow-Rate"

t	time since injection of particles into pipe, T
$T(x)$	function in equation (3-11)
u_r, u_θ, u_x	velocities (laminar) in r, θ and x directions, LT^{-1}
u	point velocity of gas in axial direction, LT^{-1}
U	average velocity of gas, LT^{-1}
u^*	friction velocity $= \sqrt{\frac{\tau_w g_c}{\rho}}$, LT^{-1}
u^+	dimensionless velocity = u/u^*
u_p	particle velocity in direction of flow, LT^{-1}
v_p	particle velocity in direction of fall, LT^{-1}
v_t	terminal fall velocity of particle, LT^{-1}
$V(r)$	function in equation (3-11)
x	distance downstream of particle injector, L
y	distance from wall = R-r, L
y^+	dimensionless distance from wall = yu^*/ν
Y_o	zero-order Bessel function of second kind
z	dimensionless radial distance = r/R
W	mass flow-rate of gas, MT^{-1}
W_p	solids flow-rate, MT^{-1}

Greek Symbols

α_n	roots of $J_1(\alpha_n R) = 0$, L^{-1}
β_n	roots of $J_1(\beta_n) = 0$, dimensionless
ΔH	head of gas, FLM^{-1}
ε	fluid eddy diffusivity, L^2T^{-1}
ε_p	particle eddy diffusivity, L^2T^{-1}

ρ	gas density, ML^{-3}
ρ_p	particle density, ML^{-3}
μ	microns
μ	viscosity, $ML^{-1}T^{-1}$
ν	dynamic viscosity = ρ/μ, L^2T^{-1}
τ_w	shear stress at wall, FL^{-2}

Subscripts

$\bar{\ }$	bar denotes time-mean value
$(\ )'$	turbulent fluctuation component

1. INTRODUCTION

The transport of solid particles in a fluid medium is of interest in many fields of engineering. This interest is manifested in Chemical Engineering by the growing trend towards the use of finely divided solids or liquids in a number of industrial processes where the unique properties of solids-gas flow could be made to play an important role. The advantages resulting from the smallness of the particles are the ease of handling, the provision of large surface areas which give high rates of heat and mass transfer, high rate of reaction and the near absence of resistance to diffusion within particles.

In these contacting processes, normally the fluid must be moving at fairly high velocities and must be flowing turbulently in order to suspend and carry the solids. There are in general, two categories of suspensions. The first is made up primarily of particles; in many instances, the fluid-solids mixture behaves as a homogeneous fluid and exhibits non-Newtonian behaviour. Examples of this are fluidized beds and concentrated slurries. The second is that in which the solids phase exists in a dilute condition, i.e. the particles are far enough removed from one another so that they may be treated as individual particles, each individually contributing to the overall character of the flow. Operations involving such dilute suspensions are termed pneumatic systems; examples here are spray drying, flash drying, atomized suspension technique, mist-annular flow in two-phase gas-liquid flow etc.

In spite of much activity relating to particle mechanics in associated fields(e.g. fluidized beds), our understanding of the actual nature of pneumatic systems is at present not far advanced. The design of equipment in which a dilute suspension of particles in a gas is to be conveyed, requires an adequate knowledge of the diffusion of both fluid and solid particles in the turbulent gas stream. As will be shown later, if one has knowledge of the eddy diffusion coefficient for particles at each point in a turbulent gas stream, in principle the motion of each particle can be described and its location at any time can be ascertained.

One of the most recent studies on gas diffusion was made by Koo (1,2). His experiment was carried out in a horizontal pipe of 5.5 in. inside diameter and approximately 32 ft. long. The objective of this research program is to extend Koo's work by using his experimental apparatus for investigating the eddy diffusion of solid particles.

Although great accuracy is not claimed for the data obtained in this study because of some inherent difficulties with using Koo's equipment, the results obtained here do give a fairly good picture of the motion of particles in turbulent pipe flow.

It was expected at the outset that this work could only be started, and additional studies would be required to complete the investigation of the full range of variables in this complex particles - gas flow system.

2. LITERATURE REVIEW

The understanding of particle transport requires a knowledge of the turbulent motion and the relationship between the gas motion and the particle motion. A survey on the diffusion of gases is therefore useful before studying the diffusion of particles.

2.1 Eddy Diffusion of Gases in a Turbulent Field

Eddy diffusion is the term which is applied to describe the transport of suspended or dissolved material by a turbulent mixing process. The turbulence is characterized by the random motion of the particles or of aggregates of such particles which constitute the fluid stream. The irregular motion of the fluid manifests itself by the formation of eddies, i.e. small masses of fluid moving temporarily as a unit.

Eddies transfer finite quantities of material from one point to another as a result of their relative motion with respect to the main body of the stream. Such terms as "intensity of turbulence" and "scale of turbulent motion" are used to quantitatively describe turbulent motion in statistical theories of turbulence (3).

As will be shown in Chapter 3, a mathematical model, which describes the mass transfer in turbulent flow, may be written as follows:

$$N = - (D + \varepsilon) \frac{\partial \bar{C}}{\partial y} \qquad (2\text{-}1)$$

where N is the rate of material transfer per unit area, $\frac{\partial \bar{C}}{\partial y}$ is the mean concentration gradient in the direction of diffusion, D and ε are the

coefficients of molecular diffusion and turbulent diffusion respectively.

The coefficient of turbulent diffusion or the eddy diffusivity is primarily a function of flow condition. Two other quantities useful in dealing with transport phenomena in turbulent flow are eddy viscosity for momentum transfer and eddy conductivity for heat transfer. They are related to the shear stress and the heat flux respectively in the form similar to equation (2-1). It is accepted that the eddy diffusivity is closely analogous to the eddy conductivity (3) and some simple analogy is usually considered to exist between the eddy conductivity and eddy viscosity (4,5). Therefore, the value of one coefficient, either for mass, heat or momentum transfer, may be expected to give some indication on the transport of two remaining modes. For a turbulent air flow, it has been found by many investigators that the ratio between eddy diffusivity and eddy viscosity is in the range of 1.0 to 1.6.

Since fluid flow has been studied much more than either heat or mass transfer,many semi-empirical equations have been proposed for determining the coefficient of momentum transfer. The equation of Gill and Scher (6) has the advantage of describing the eddy viscosity over the entire flow, in contrast to earlier expressions of Von Karman (5), Lin et al. (7), Deissler (9) etc. Further details concerning the analogy described above can also be found in the literature review made by Koo (1).

For experimental measurements of the gas diffusion, the gas tracer technique has been widely used in many studies reported in the literature (1, 2, 10, 13, 14, 16, 18, 20, 29, 30). This technique

consists of injecting a foreign gas into a turbulent stream and measuring the concentration of the gas tracer at various radial and axial positions downstream from the point of injection. The diffusion coefficient is then calculated by solving the diffusion equation. This technique was used by Koo (1) and is employed in the present study; it will be discussed in detail in Section 3.

Towle and Sherwood (10) used the point source solution derived by Wilson (11) to correlate their data on the mass transfer of carbon dioxide in a turbulent pipe flow. By using Wilson's equation, they were assuming that the turbulence is constant in the central core of the flow.

Sherwood and Woertz (12) reported results on the diffusion of water vapour between parallel plates. They found that the eddy diffusivity is nearly constant in the turbulent core.

Flint et al.(14) studied the diffusion of hydrogen and carbon dioxide in air and that of potassium chloride in water. They plotted the dimensionless group $\varepsilon/2RU$ versus the Reynolds number, and found that there was good agreement between their results for air and for water. This suggested that the above correlation could be used for other systems. From this work, the dimensionless $\varepsilon/2RU$, decreases with Reynolds number up to 50,000; however, the increasing of $\varepsilon/2RU$ with higher Reynolds number is not expected.

Various theoretical aspects of material transfer were discussed by Klinkenberg et al. (15), Schlinger and Sage (16) and Taylor (17, 18). The latter has introduced the statistical theory of diffusion which was

adopted by a number of investigators (13, 14, 20).

Several other experimental studies have also been made to clarify the question of gas diffusion in different flow systems (19, 20, 28, 29, 30). As indicated earlier, the most recent work is that of Koo (1,2) who investigated the mass transport of ethylene in a turbulent air stream at 4 Reynolds numbers varying from 7300 to 58300. His results were expressed in terms of the non-dimensional diffusivity ε/u^*R versus radial position. The average profile at 4 Reynolds numbers is included in Figure 2-1, in comparison with that obtained by Reichardt (8) for eddy viscosity and by Johnkand Hanratty (21) for eddy conductivity. Koo's average value ($\varepsilon/u^*R=0.07$) over the pipe radius, was transformed by the author to ε/UR versus Reynolds number in order to be compared with the average values of other workers (Figure 2-2).

2.2 Eddy Diffusion of Solid Particles in a Turbulent Field

The above literature review on turbulent gas diffusion showed that one can estimate the gaseous eddy diffusivity with reasonable confidence from available data or from analogy between heat, mass and momentum transfers. However, this coefficient is not adequate to describe the motion of solid particles or liquid droplets. The transport of solid and fluid particles can be expected to differ because of their different inertia effects.

The diffusion of particles in turbulent streams has been the object of many investigations. Unfortunately, because of the complex nature of turbulent motion, some quite contradictory results have been observed. The works of Alexander and Coldren (22) on the dispersion of liquids droplets (average diameter of 27 microns), Kesler (23) on the movement of atomized

FIGURE 2-1

TYPICAL EXPERIMENTAL PROFILES

FOR COEFFICIENTS OF HEAT, MASS

AND MOMENTUM TRANSFER

CURVE	COEFFICIENT	REFERENCE
1	Heat	JohnK & Hanratty(21)
2	Mass	Koo (1)
3	Momentum	Reichardt (8)

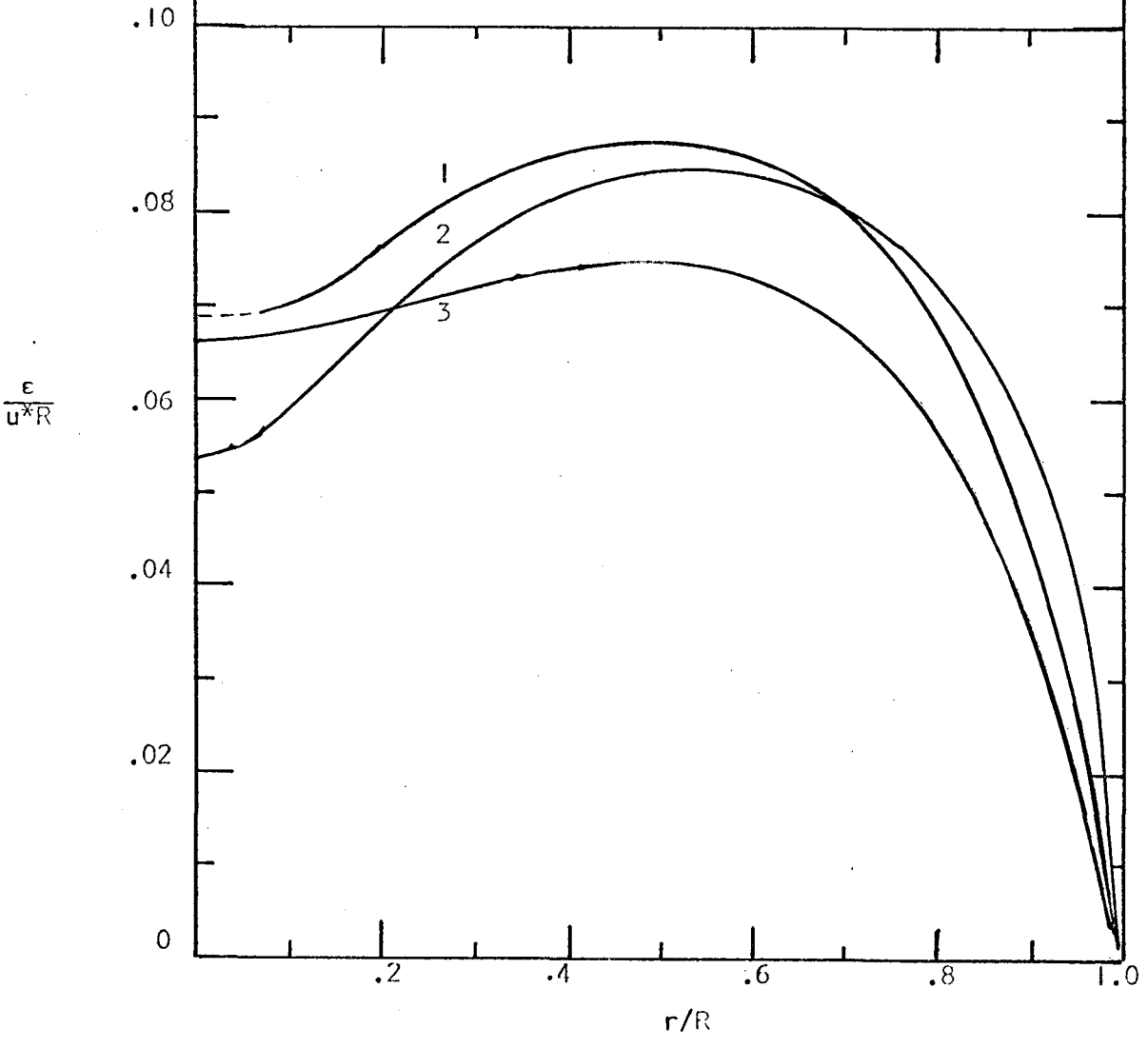

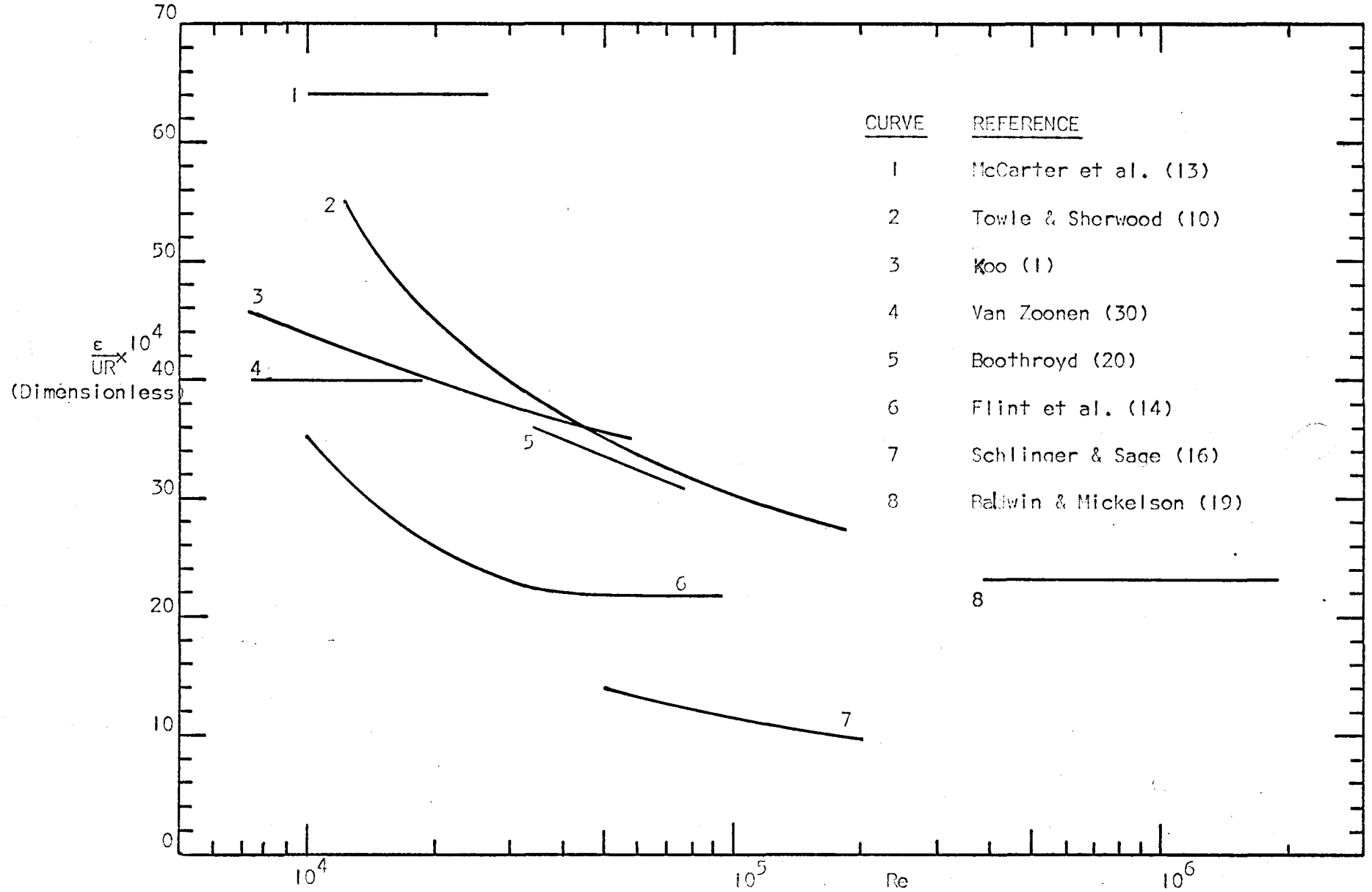

FIGURE 2-2 CORRELATION OF DATA ON GAS DIFFUSION COEFFICIENT

sprays (14 to 30 microns), Soo (24) on the statistical study of the momentum transfer in a turbulent fluid indicated that the diffusivity of particles was approximately equal to that of the carrier stream. This is in contradiction with latter theoretical studies of Soo (25), Peskin (26), Rouhiainan and Stachiewicz (27) and experimental works of Soo (28) and Farmer (29) which showed the effects of particle - particle and particle-fluid interaction in two-phase flow systems.

Soo (25) presented in his book (Chapter 2) an equation for $\varepsilon_p/\varepsilon$ (ratio of particle diffusivity to fluid diffusivity) in terms of Lagrangian and Eulerian microscales of turbulence and of particle Reynolds number. Rouhiainen and Stachiewicz (27) suggested that the assumption of equality of particle and fluid diffusivity is only valid for submicron particles, and becomes completely untenable under most actual conditions. These authors also derived a method of calculating the dependence of the ratio $\varepsilon_p/\varepsilon$ on Reynolds number, based on the integration of turbulent energy spectra.

In his paper, Soo (28) reported data on the diffusion of helium and of glass particles in a turbulent air stream flowing in a square duct of 3 in. x 3 in. in cross section and 21 ft. in length. The two size ranges of glass beads used were 105 to 125 microns and 210 to 250 microns, and the range of particle loading was up to 0.06 lb. of solid per lb. of air. The gas phase turbulent motion was determined by the gas tracer technique and the motion of solid particle was observed by a photo-optical technique. For the density ratio of particle to stream equal to 1780 in this experiment, the value of $\varepsilon_p/\varepsilon$ was found to be much smaller than 1, to the order of 10^{-2} to 10^{-1}.

The investigation of Farmer (29) was somewhat more elaborate. This work involved the measurement of mass transport coefficients of fluid (water) and solids (spherical resin beads, 460 microns in diameter and 1.31g/cc in density)in a closed chamber of 22.4 in. in length and 6 in.x 1 in. in cross section. The eddy diffusion of fluid was observed by injecting a liquid dye into a turbulent field. Dye concentration was determined by measuring light transmission through the chamber. In the case of solid diffusion, the solids were used as tracer and particle concentration was performed by tagging ion-change resin beads with radioactive cesium and measuring the count rate at various elevations in the fluid. Farmer found the ratio $\varepsilon_p/\varepsilon$ equal to 0.67 with insignificant change with Reynolds number.

Van Zoonen (30),on the other hand, studied the diffusional phenomena of air and cracking catalyst of size ranging from 20 to 150 microns, in a vertical riser of 5 cm in diameter and 10m high. Cracking catalyst tagged with about 5% wt of ammonium chloride was used as tracer. The gas solids samples obtained in the test section were each weighed and then mixed with a known amount of water to dissolve the ammonium chloride into the water. The relative concentrations of ammonium chloride were obtained by measuring the relative electric conductivity of these solutions. Van Zoonen reported that the dimensionless dispersion coefficient ε/UR was $(40 \pm 10) \times 10^{-4}$ for air alone,$(30 \pm 10) \times 10^{-4}$ for air with the present of solids and $(20 \pm 10) \times 10^{-4}$ for solid particles.

The problem of particle diffusion has also been investigated experimentally by Rouse (31), Kalinske and Pien (32), Longwell and Wess (33),

and Soo (34, 35) in different types of flow systems. The data of Kalinske and Pien and those of Rouse for combined eddy diffusion and setting of sand particles in water indicated little variation of diffusivity with particle size. Longwell and Weiss (33) were interested in the initial spray injected at the centre of a turbulent pipe flow. Soo (35) reported that his results for particle diffusion coefficient were of the same order of magnitude as that found by Van Zoonen (30).

This summary of previous work on the diffusion of solid particles in turbulent streams illustrated the need of data on these subjects and showed that a comparison between the transport of solid and fluid particles is very difficult unless they are examined in the same turbulent environment. This is the reason the decision was made to use Koo's equipment and extend his work to the present study of the turbulent diffusion of solid particles.

3. DIFFUSION EQUATIONS IN TURBULENT PIPE FLOW

This chapter presents an analysis of the diffusion of a component from a small source (i.e. tracer technique) in a gas flowing turbulently in a cylindrical duct.

The differential mass balance in cylindrical coordinates for the steady-state flow of a laminar incompressible fluid with no chemical reactions is:

$$u_r \frac{\partial C}{\partial r} + u_\theta \frac{\partial C}{\partial \theta} + u_x \frac{\partial C}{\partial x} = \frac{1}{r}\frac{\partial}{\partial r}\left(Dr \frac{\partial C}{\partial r}\right) + \frac{1}{r^2}\frac{\partial}{\partial \theta}\left(D \frac{\partial C}{\partial \theta}\right) + \frac{\partial}{\partial x}\left(D \frac{\partial C}{\partial x}\right) \qquad (3\text{-}1)$$

For the case of turbulent flow the concentration and each of the velocities in the above equation may be replaced by the sum of a time-mean value and a fluctuating component, i.e., $(\bar{u} + u')$ would be substituted for u and $(\bar{C} + C')$ for C. Assuming radial symmetry, a fully-developed velocity profile and constant fluid properties, and neglecting the diffusion in axial direction, the differential equation for turbulent mass transfer simplifies to:

$$\bar{u}_x \frac{\partial \bar{C}}{\partial x} = \frac{D}{r}\left[\frac{\partial}{\partial r}\left(r \frac{\partial \bar{C}}{\partial r}\right)\right] - \frac{1}{r}\frac{\partial}{\partial r}\left(r\overline{u_r' C'}\right) \qquad (3\text{-}2)$$

where $\overline{u_r' C'}$ describes the turbulent mass flux designated by N_t.

The terms on the right side of equation (3-2) represent the molecular and turbulent contributions, respectively, to radial diffusion. The second term can be given a form identical to the first by introducing the following

definition of the eddy diffusivity ε:

$$N_t = - \varepsilon \frac{\partial \bar{C}}{\partial r} \tag{3-3}$$

which is analogous to Fick's law of molecular diffusion:

$$N_\ell = -D \frac{\partial \bar{C}}{\partial r} \tag{3-4}$$

Thus equation (3-2) becomes:

$$u \frac{\partial C}{\partial x} = \frac{1}{r} \frac{\partial}{\partial r} \left[r (D + \varepsilon) \frac{\partial C}{\partial r} \right] \tag{3-5}$$

For convenience the bars over the velocity and concentration, and the subscript x on the time-mean point velocity $\bar{u}_x$ have been dropped.

In turbulent region, the molecular diffusivity, D, is small in comparison with the large value of ε and so it can be neglected.

It is obvious from equation (3-5) that one can determine ε if the concentrations at various radial and axial positions, and the velocity profile u are known from experimental measurements. Many different methods have been developed to solve for ε. If one is interested to obtain ε as a function of r, the following expression is used:

$$\varepsilon(r) = \frac{\partial}{\partial x} \int_0^r Curdr \Big/ r \frac{\partial C}{\partial r} \tag{3-6}$$

which can be calculated by appropriate graphical integrations and differentiations or by numerical techniques. The first technique was used by JohnK and Hanratty (21) who solved the similar equation for heat transfer, and the second was adopted by Koo (1). Their results were shown in Figure 2-1.

A simpler method which has been used by many other authors (10, 16, 20, 22, 23, 30, 33) and is being employed in the present study, is to find an approximate analytical solution of equation (3-5) by assuming ε and u are constant over the pipe radius. Thus equation (3-5) reduces to:

$$\frac{\partial^2 C}{\partial r^2} + \frac{1}{r}\frac{\partial C}{\partial r} = \frac{U}{\varepsilon}\cdot\frac{\partial C}{\partial x} \qquad (3\text{-}7)$$

which, in conjunction with suitable boundary conditions can be solved analytically.

Experimentally, a foreign gas may be injected, isokinetically into a pipe carrying a turbulently flowing gas stream. Analysis downstream at various radial and axial locations allows one to trace the diffusion of the gas in the flowing stream. Similarly, a particle-laden gas stream may be injected and the concentration of particles measured downstream. Under these conditions, the boundary conditions are:

$$x = 0 \qquad C = f(r) \qquad (3\text{-}8)$$

$$\text{with} \quad C = C_\infty \frac{R^2}{b^2} \quad \text{for } o \leq r \leq b \qquad (3\text{-}8a)$$

$$\text{and} \quad C = 0 \quad \text{for } b \leq r \leq R \qquad (3\text{-}8b)$$

$$r = R \qquad \frac{\partial C}{\partial r} = 0 \qquad (3\text{-}9)$$

$$r = 0 \qquad C \text{ is finite} \qquad (3\text{-}10)$$

Note that the concentration of the tracer is assumed to be uniform over the cross-section of the injector tube (radius b). Equation (3-8a) follows from a material balance assuming the tracer spreads uniformly into the gas stream at a large distance from the injector, i.e.,

$$C_\infty = \lim_{x \to \infty} C \qquad \text{for all } r$$

which is given by the ratio of tracer to gas flow rates.

Equation (3-7) can be solved by the method of separation of variables.

Let

$$C(r, x) = V(r) \cdot T(x) \tag{3-11}$$

Substitution of this trial function into equation (3-7) gives:

$$\frac{1}{V}\frac{d^2V}{dr^2} + \frac{1}{rv} \cdot \frac{dV}{dr} = \frac{1}{Ta} \cdot \frac{dT}{dx} \tag{3-12}$$

where

$$a = \varepsilon_p / U \tag{3-12a}$$

The subscript p is now used to designate the particle.

The left side of equation (3-12) is a function of r alone, and the right side is a function of x alone. This can be true only if both sides are equal to a constant, say $-\alpha^2$.

The problem then becomes one of solving two equations. The first being:

$$\frac{1}{Ta} \cdot \frac{dT}{dx} = -\alpha^2 \tag{3-13}$$

and having a solution:

$$T = K \cdot e^{-\alpha^2 a x} \tag{3-14}$$

The second is:

$$\frac{d^2V}{dr^2} + \frac{1}{r} \cdot \frac{dV}{dr} + \alpha^2 V = 0 \tag{3-15}$$

which is a Bessel equation of zero order. The solution of this equation can be written - see for example, Jenson and Jeffreys (36)- as:

$$V = AJ_o(\alpha r) + B\,Y_o(\alpha r) \quad \text{if } \alpha \neq 0 \tag{3-16a}$$

or

$$V = A' + B' \ell nr \quad \text{if } \alpha = 0 \tag{3-16b}$$

Since $Y_o(0) = -\infty$ and $\ell n(0) = -\infty$, boundary condition (3-10) asserts that $B=B' = 0$.

Because $C = V.T$, the solutions of equation (3-7) are:

$$C = A' \quad \text{if } \alpha = 0 \tag{3-17a}$$

$$C = A_\alpha J_o(\alpha r) e^{-\alpha^2 ax} \quad \text{if } \alpha \neq 0 \tag{3-17b}$$

The most general solution of equation (3-7) is therefore obtained by adding all permissible particular solutions together. Thus:

$$C = A' + \sum_{n=1}^{\infty} A_n J_o(\alpha_n r) e^{-\alpha^2 ax} \tag{3-18}$$

when x tends to infinity, the second term tends to zero, hence:

$$A' = C_\infty \tag{3-19}$$

The boundary condition (3-9) indicates that the derivative of equation (3-18) with respect to r is zero at r = R. This gives:

$$J_1(\alpha_n R) = o \tag{3-20}$$

i.e. $\alpha_n R$ are roots of the Bessel function of the first kind of zero order.

Now from condition (3-8), and equation (3-19), we have:

$$f(r) = C_\infty + \sum_{n=1}^{\infty} A_n J_o(\alpha_n r) \tag{3-21}$$

it being assumed that f(r) can be expanded in a series of Bessel function of zero order. The A_n's are determined by multiplying both sides of equation (3-21) by $rJ_o(\alpha_m r)$ and integrating from 0 to R:

$$\int_0^R f(r)\, r\, J_o(\alpha_m r)\, dr = C_\infty \int_0^R r\, J_o(\alpha_m r)\, dr + \sum_{n=1}^{\infty} A_n \int_0^R J_o(\alpha_n r)\, J_o(\alpha_m r)\, dr \quad (3\text{-}22)$$

It is simpler to evaluate the terms of the above expression separately. The first term becomes:

$$C_\infty \int_0^R r\, J_o(\alpha_m r)\, dr = C_\infty \; R \frac{J_1(\alpha_m R)}{\alpha_m} = 0 \quad (3\text{-}23)$$

from result (3-20).

Taking a general term with $n \neq m$ from the infinite sum:

$$A_n \int_0^R J_o(\alpha_n r)\, J_o(\alpha_m r) r dr = \frac{A_n R}{\alpha_n^2 - \alpha_m^2}\left[\alpha_n J_o(\alpha_m R) J_1(\alpha_n R) - \alpha_m J_o(\alpha_n R) J_1(\alpha_m R)\right] = 0 \quad (3\text{-}24)$$

again from result (3-20).

For the special term in the series when $n = m$, we have:

$$A_n \int_0^R J_o^2(\alpha_n r) r dr = A_n \frac{R^2}{2}\left[J_o^2(\alpha_n R) + J_1^2(\alpha_n R)\right] = A_n \frac{R^2}{2} J_o^2(\alpha_n R) \quad (3\text{-}25)$$

Substituting equations (3-23), (3-24), and (3-25) into (3-22) gives:

$$A_n = \frac{2 \int_0^R f(r)\, r\, J_o(\alpha_n r)\, dr}{R^2 J_o^2(\alpha_n R)} \quad (3\text{-}26)$$

With the values of $f(r)$ given by equations (3-8a) and (3-8b), the above expression becomes:

$$A_n = \frac{2\int_0^b C_\infty \frac{R^2}{b^2} r J_o(\alpha_n r)dr}{R^2 J_o^2(\alpha_n R)}$$

$$= \frac{2C_\infty}{b^2 J_o^2(\alpha_n R)} \left[r \frac{J_1(\alpha_n r)}{\alpha_n} \right]_0^b$$

$$= \frac{2 C_\infty J_1(\alpha_n b)}{b \alpha_n J_o^2(\alpha_n R)} \qquad (3\text{-}27)$$

Defining $\beta_n = \alpha_n R$ and introducing the value of A_n into equation (3-19), yields the final desired solution:

$$\frac{C}{C_\infty} = 1 + \frac{2R}{b} \sum_{n=1}^{\infty} \frac{J_1(\beta_n \frac{b}{R}) J_o(\beta_n \frac{r}{R}) e^{-\beta_n^2 \frac{\varepsilon_p}{U} \frac{x}{R^2}}}{\beta_n J_o^2(\beta_n)} \qquad (3\text{-}28)$$

The above expression shows that the coefficient ε_p depends on the relative concentration C/C_∞, rather than absolute concentration C. Therefore, the tracer rate may be changed from one run to the next, but it must be kept constant in a single run. This is the principle of the apparatus developed in the present work (Chapter 4).

The application of equation (3-28) to determine the particle diffusivity will be shown in Chapter 7.

4. EQUIPMENT

The experimental technique, the design of equipment and the operations of individual units are discussed in the following paragraphs.

4.1 General

The main apparatus used by Koo (1) in his study of diffusion of gases in fully-developed pipe flow was made available for this work. As shown in Figure 4-1, it consists of a 32 ft. length of horizontal clear acrylic pipe with a nominal inside diameter of 5.5 in. Air was drawn through the pipe by a variable speed exhaust fan, and the entrance and length of the pipe ensures that fully-developed turbulent flow exists at the diffusion section. The tracer particles (glass beads in this case) are pneumatically conveyed into the centre of the pipe in a 1/4 in. O.D. tube; a special feeder ensures that the concentration remains uniform with time. A isokinetic sampling probe, 0.175 in. I.D., is located at any one of eight sampling stations, 12 in. apart, located down the pipe. The probe may be set at any radial position at these stations. The solids are removed from the sampling line by filtration; from sampling air flow, sample weight and particle-size distribution, concentration of particles may be obtained. The majority of the glass beads are removed in a cyclone located in a 3-ft. cube air box located immediately upstream of the fan inlet.

The range of variables studied was:

Air Reynolds number = 52800

Solids-gas loading: $W_p/W \leq 0.008$

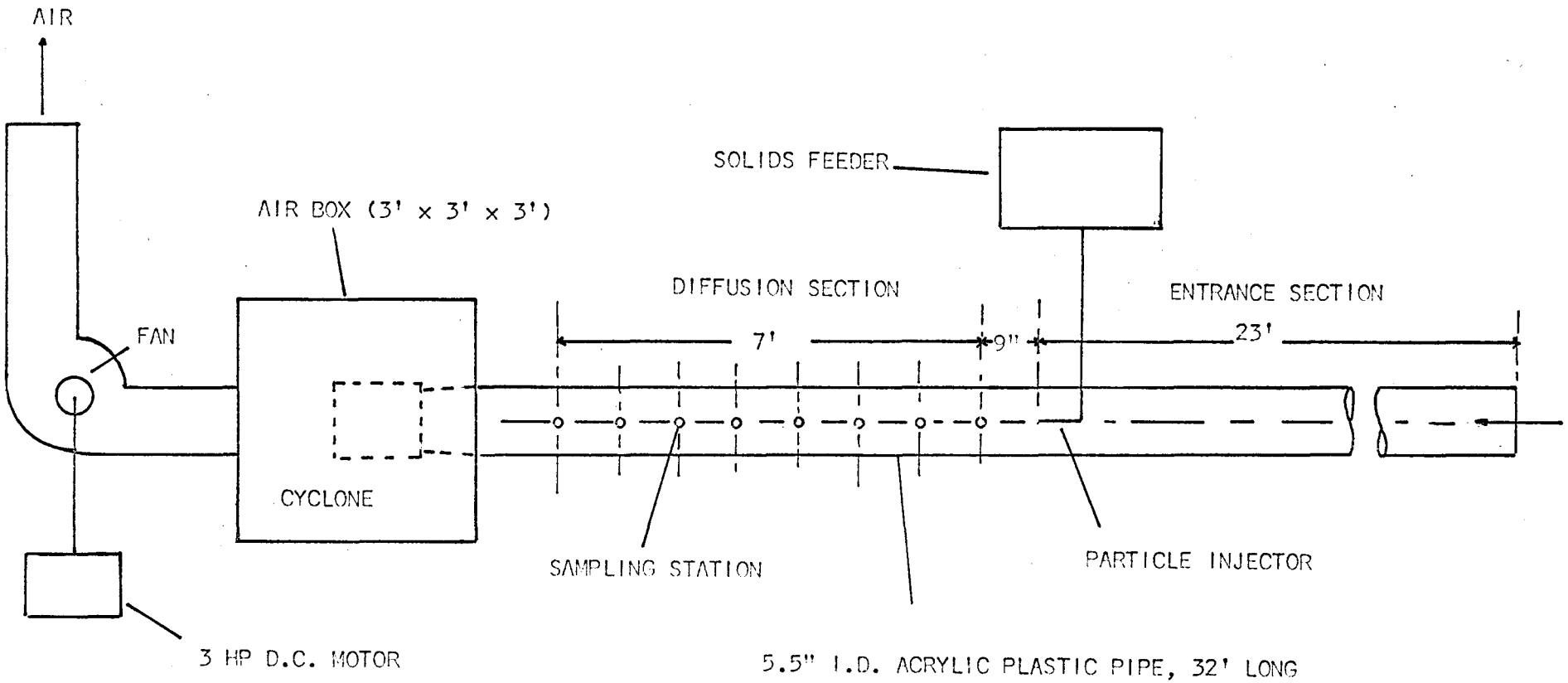

FIGURE 4-1 SCHEMATIC DIAGRAM OF PIPE INSTALLATION

Glass particles:

Volume average diameter = 35 μ

Standard deviation = 11 μ

(From normal distribution: Figure 4-2)

It was assumed that with this low solids-gas loading, the turbulence (28) and the air velocity (28, 37) are not affected by the presence of solids.

The detailed description of the equipment follows:

4.2 Solid Particles

The solid particles used in this work were glass beads, Type 500, provided by 3M Company (St. Paul, Minnesota, U.S.A.). They are spherical in shape and have a density of 2.55g/cc. Measurement of particle size distribution was made by microscopic methods and based on a sample of 1540 particles. Photographs of these particles were taken and enlarged at a total magnification of 60, and the images of the individual particles were counted and classified with a Carl Zeiss Type TGZ3 Particle Size Analyser.

4.3 Solids Feeder

4.3.1. Development of Feeder

The feeding of solids at a constant rate into the flowing air presented many difficulties.

The first design of the solids feeder was a rotary valve equipped with a variable speed motor and connected to the bottom of a solids hold-up tank. Each revolution of the rotor discharged some volume of solids. It was observed that the solids flowrate pulsed as each section of glass beads rotated into the discharge. This variation in concentration was deemed

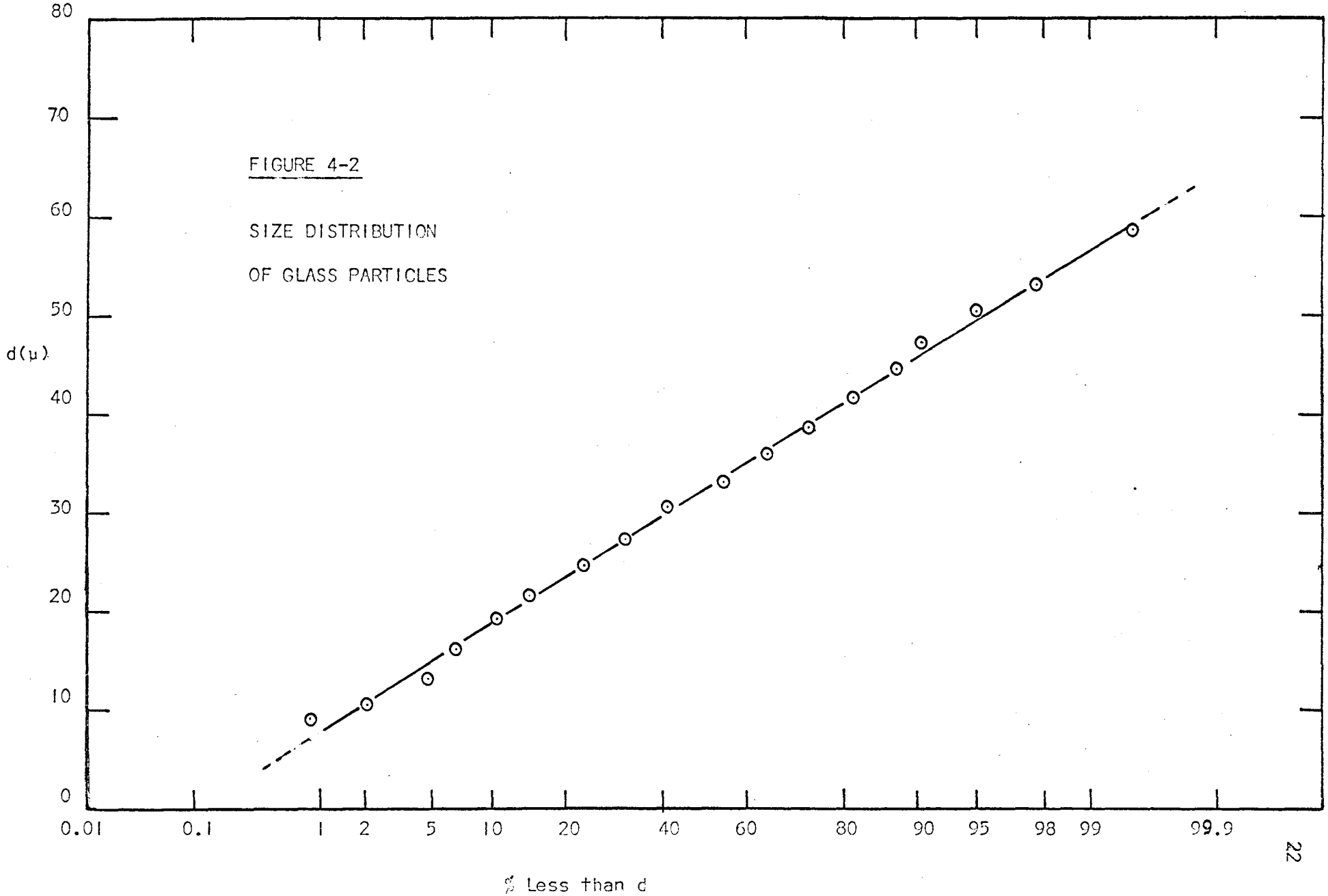

FIGURE 4-2

SIZE DISTRIBUTION

OF GLASS PARTICLES

unsatisfactory.

A second method was then suggested to fasten an electrical vibrator (with variable amplitude) to the solids hold-up tank. Vibrating the apparatus kept the solids flowing through a 3/32 in. diameter orifice located at the bottom of the hold-up tank. Preliminary tests showed that the solids discharged continuously from the above system but with a rate which depended sensibly on the height of solids in the tank. This suggested that the solids height should be kept constant by feeding continuously from the rotary valve system into the solids tank associated with the orifice feeder. Figure 4-3 indicates the complete solids feeding system. The feed to the lower tank can be adjusted to maintain a constant height by varying the rotary valve speed. The vibrator ensures uniform flow from the orifice. It was found that the transportation of solids into the pipe could be better achieved by introducing a small amount of air into the free space of the lower solids hold-up tank.

4.3.2. Detailed Description

Each component of the solids feeder is discussed below:

The upper tank, made from a copper sheet, consists of a box (9 in. high by 4 in. by 5 in.); a cone (3 1/2 in. high) was located on the bottom; a flange connects it to the rotary valve; a glass window fixed on the side of the tank over most of its height, allows the solids level to be observed.

The rotary valve, as illustrated in Figure 4-4, has the following components:

- rotor and shaft (brass)
- seal plates (brass)
- ball bearings

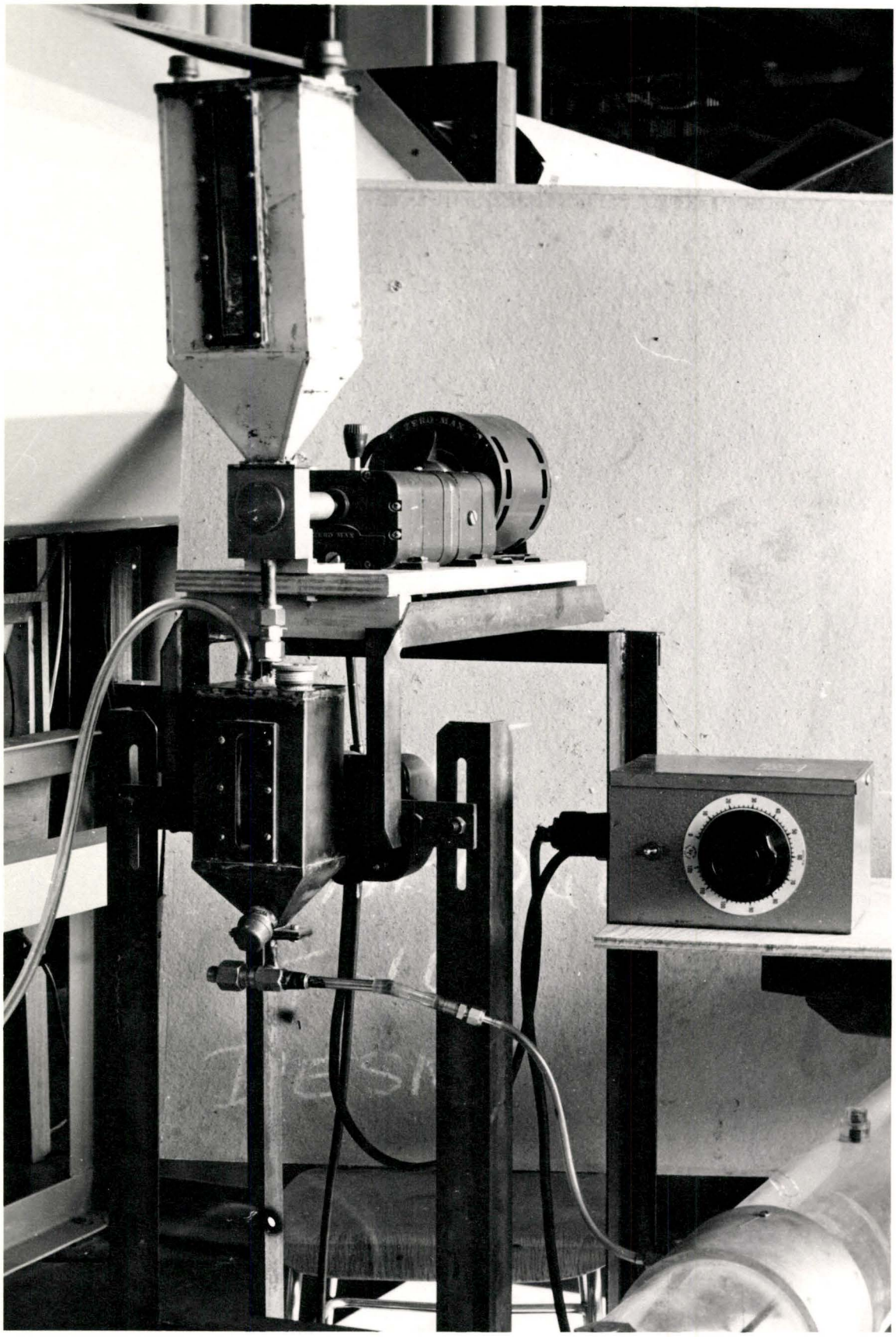

FIGURE 4-3 PARTIAL VIEW OF SOLIDS FEEDER

- body (brass)
- end caps (brass)
- coupling (aluminum)
- Zero-max variable-speed drive (The Zero-Max Co., Minneapolis, Minn. 55408, U.S.A.).

The valve rotor is 0.992 in. diameter and 1/4 in. wide. Fifteen slots, 1/8 in. wide and 1/16 in. deep, running parallel to the axis of the rotor, are machined around the periphery of the rotor. A shaft of 0.335 in. diameter and 3 1/2 in. long connects the rotor to the Zero-Max unit. Each end of the rotor is followed by a 3/32 in. seal plate and a 3/8 in. ball bearing. The purpose of these seal plates is to prevent the dust entering the bearings.

The above components are contained in a body of dimensions 3 1/2 in. x 2 1/2 in. x 1 in. Two end caps are fixed at the ends of the body to seal the unit. The clearance between the edges of the rotor and the valve body is about 0.087 in.

The valve shaft is connected to the variable speed drive by an aluminum coupling. The speed range of the Zero-Max. speed controller is 0 to 110 r.p.m.

The solids from the upper tank enter the valve body through a cross section of 1 in. x 1/2 in. and are discharged to the lower tank through a 1/2 in. copper tube.

The lower tank, made by copper is a 6 in. high by 4 in. by 3 in. box on top of a 2.5 in. high cone which has an opening of 1/2 in. x 1/2 in. at the bottom. A glass window on the front of the tank allows the solids

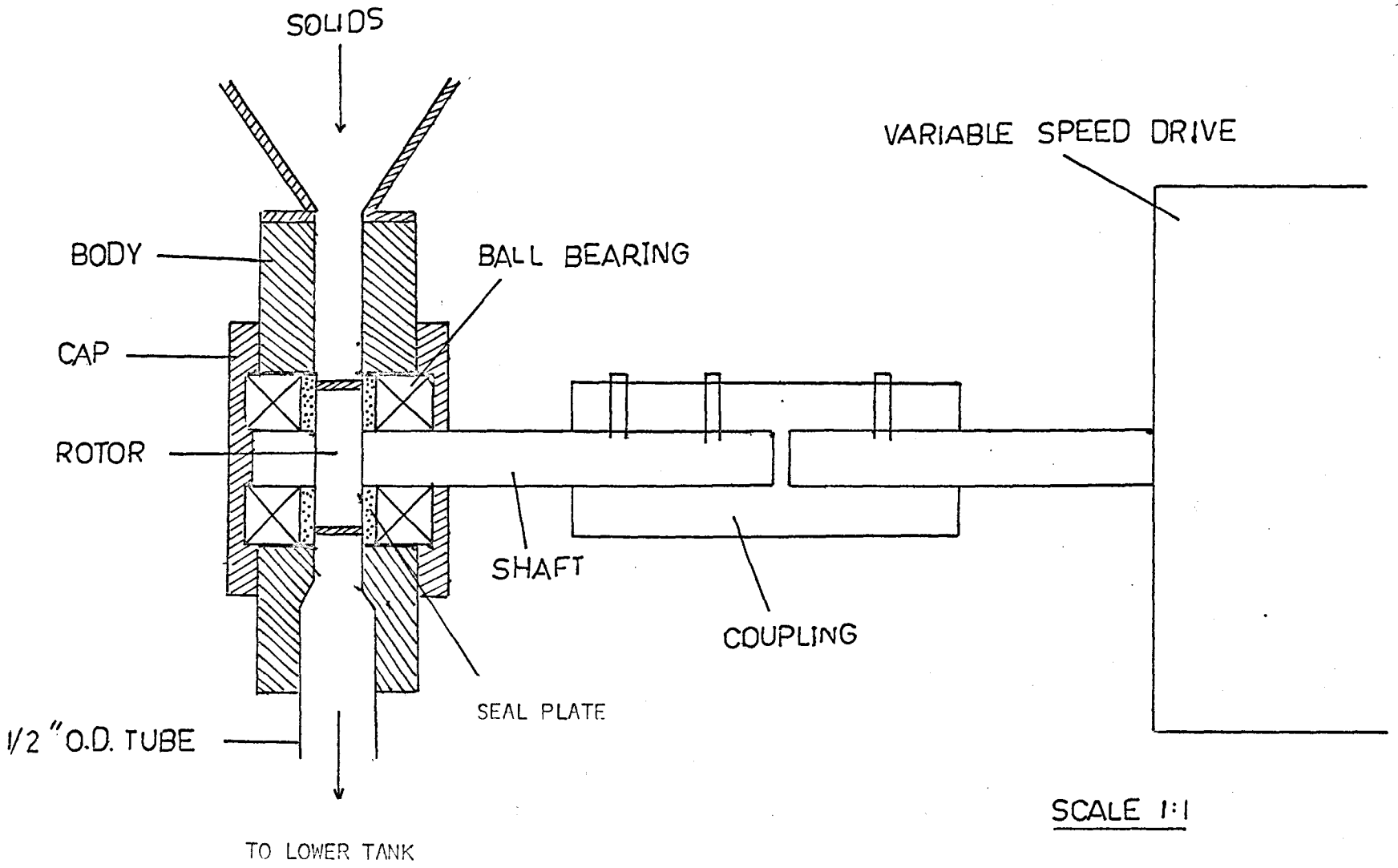

FIGURE 4-4 ROTARY VALVE

level to be observed.

The electric vibrator (Model V.9 - Ser. A.7199, Syntron Canada Limited) is located at the back of the above tank and at approximately 4 in. from the top. It is connected to a support brass plate (inside the tank) and a 12 in. long horizontal steel bar, which is, in turn, connected to an angle steel frame system fixed on the floor as can be seen in Figure 4-3.

The amplitude control for the vibrator is accomplished by a variable auto-transformer (Model C-R3, Ser. G61C8487, Syntron Canada Limited) with voltage ranging from 0 to 120 volts.

The bottom of the tank is flanged connected to a thin orifice plate. The solids leaving the orifice enter the throat of a venturi through which the conveying air passes (Figure 4-5). The plate was made from a 2 1/2 in. x 1 in. aluminum plate, 1/32 in. thick. The orifice bored at the centre of the plate was carefully machined so that it was burr-free. The flow of the conveying air is controlled by a needle valve; its rate is measured by a rotameter (Fisher and Porter Canada Limited, FP 1/4 - 25 - G - 5/81). The solids-gas flow can be observed through a 2 in. length of 6 mm. glass tube inserted in the line between the venturi and the particle injector.

In order to prevent the upward flow of the air back from the orifice, the lower tank must be perfectly closed. The auxiliary air flow fed to the tank also helps to prevent this. This flow is controlled by a needle valve; a rotameter (Fisher and Porter Canada Limited, FP 1/8-25 - G - 5/81) indicates its magnitude.

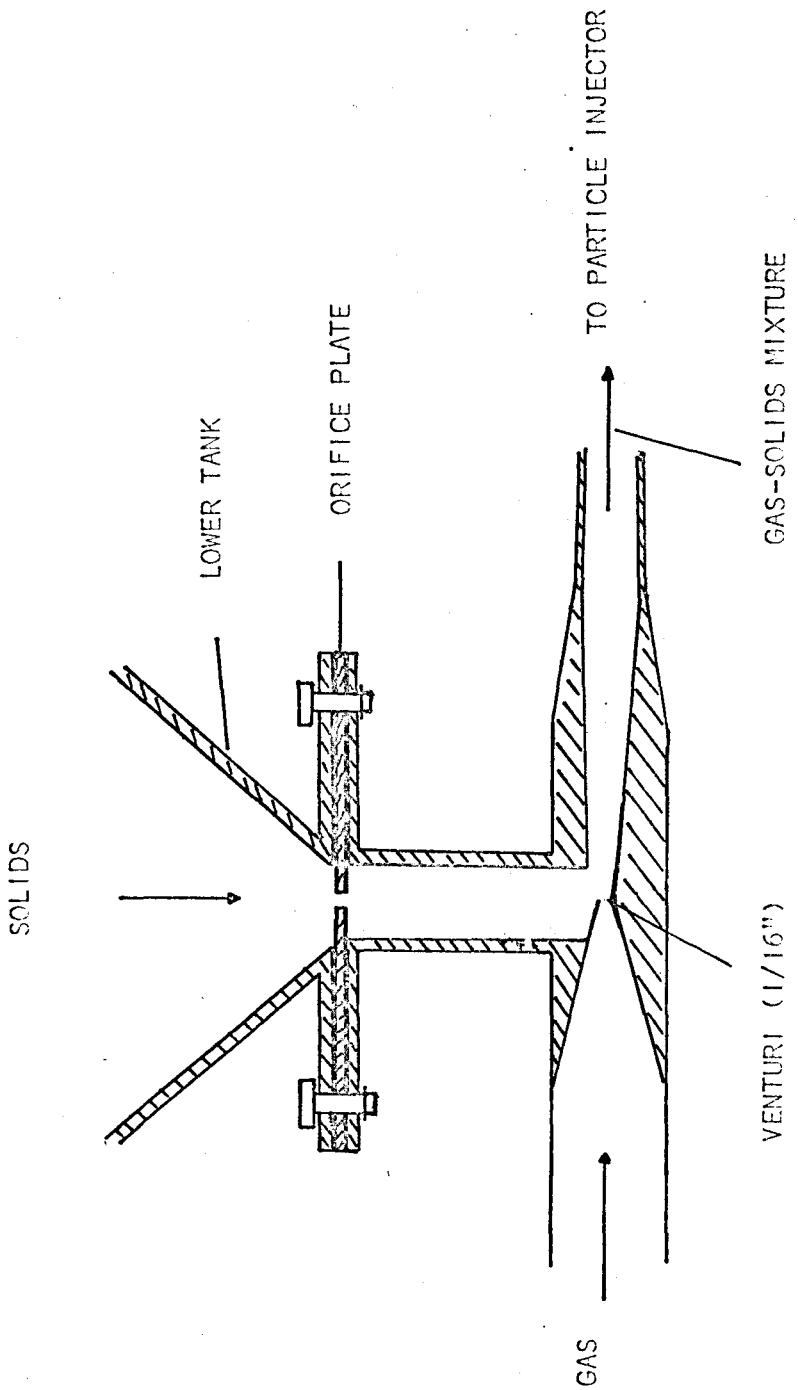

FIGURE 4-5. GAS-SOLIDS, SUSPENSION ZONE OF SOLIDS FEEDER

4.3.3 Calibration of Solids Flow-Rate (S.F.R.)

The flow-rate of solids which discharge from the solids feeder described above, depends on the following factors: orifice diameter, vibrator amplitude, solids level in the lower tank, flow-rate of the auxiliary air and humidity of solids.

Testing the uniformity of the S.F.R. was performed under conditions where the solids discharged from the orifice into the open and where they discharged from the orifice into the venturi with the conveying air flowing.

In the first case, the tests were very easy; they consist of measuring during a finite time, the weight of solids collected in a container located below the orifice plate. The following observations are noted:

-The vibrator caused excessive strain on the equipment when operated near maximum voltage. For this reason, the voltage range was restricted to 80-100 volts.

-The orifice, on the other hand, must have a diameter larger than 1/16 in. to give consistent operation.

-Preliminary tests showed that as the solids height decreased with time, the S.F.R. increased. One possible explanation is that when this height decreases, the empty space in the (lower) tank increases, therefore, the effect of vibration increases.

-If the rotary valve feeds solids to the lower tank at a rate to maintain a height variation of about $\pm$ 0.15 in. the S.F.R. stays constant to within $\pm$ 3% on the average, with some rare variations up to $\pm$ 6% in a single test, although even for the same vibrator, it may change from one test to the next as shown by curves (1) and (2) in Figure 4-6.

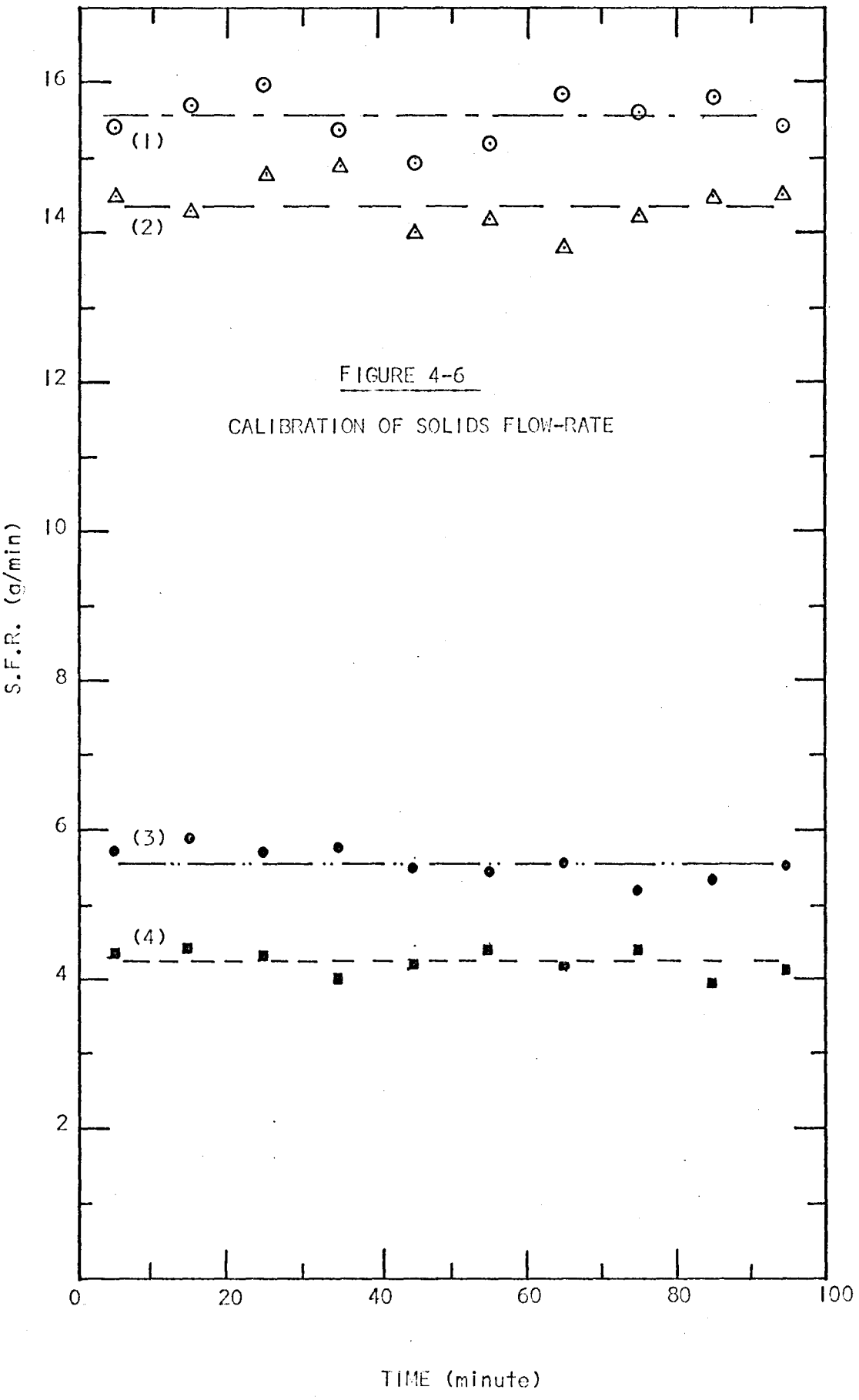

FIGURE 4-6

CALIBRATION OF SOLIDS FLOW-RATE

The situation becomes more complicated when the venturi system is connected to the orifice plate and air flows through it. The S.F.R. is much less; it was found that the auxiliary air line was necessary to facilitate the transportation of solids into the pipe. An orifice diameter of 3/32 in. was necessary to achieve the desired solids flow.

The constancy of the S.F.R. was tested by connecting a small cyclone to the outlet of the conveying tube and collecting and weighing the solids from its discharge. It was found that the upper tank must be kept relatively full of solids so that any reduction in height during the test does not affect the pressure in the lower tank. Typical experimental results are shown by curves (3) and (4) in Figure 4-6.

It is worth noting that the humidity of solids in the lower tank also reduces the S.F.R., but it does not seem to affect its uniformity.

4.4 Particle Injector.

The particle injector is located at the centre of the pipe and at an axial position approximately 23 ft. from the pipe entrance. It was made from 1/4 in. O.D. by 0.234 in. I.D. tubing and was shaped in the form of an <L> with a 9 in. length facing downstream. As shown in Figure 4-7, the injector tube is held in the centre of the pipe by a mounting plug (at pipe wall) and by three stainless steel wires located at 120^{o} intervals around the tube and 2 1/2 in. from the outlet. Each of these wires passes through a 1/64 in. hole drilled on a 5 in. long case aluminum coupling (which connects two sections of acrylic pipe) and is attached to a screw fixed on the coupling.

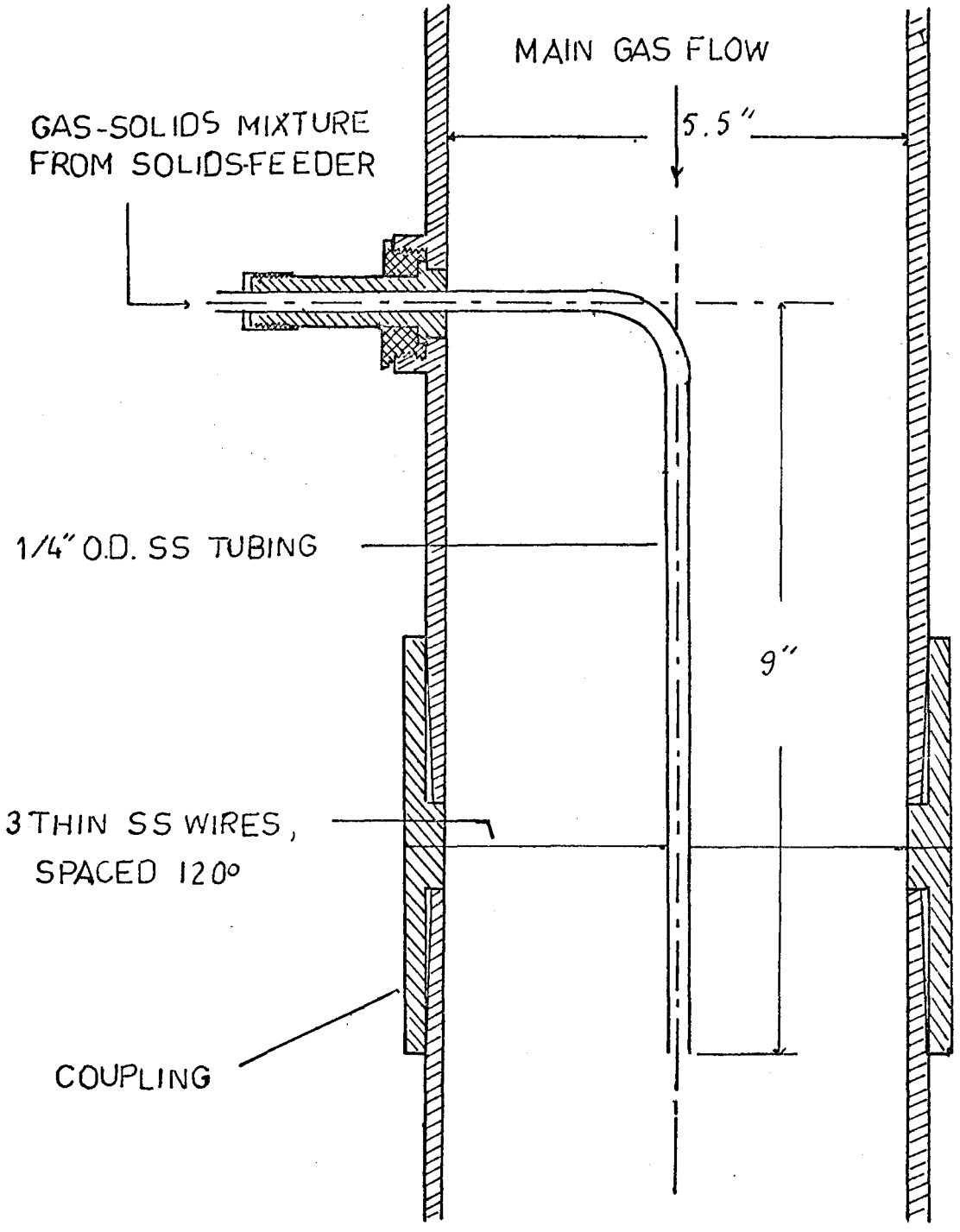

FIGURE 4-7 PARTICLE INJECTOR IN PIPE

A mark was cut on the injector tube at 2.75 in. (equal to pipe radius) from the tube centreline. The proper position of the injector was obtained by adjusting (1) the injector until this mark fitted the pipe wall (with the aid of a magnifying glass) and (2) the three wires until the injector outlet end was equidistant to the pipe wall (as measured by a micrometer).

4.5 Isokinetic Sampling of Particles

4.5.1. Introduction

In two-phase systems, need arises for drawing off a sample in such a way that the phases do not prematurely separate or change relative velocities, i.e., samples must be taken from the main stream at exactly the true flow velocity. Such a sampling method is called "isokinetic sampling". Only in this way does the probe have a 100% target efficiency.

In this study, the air velocity can be assumed unaffected by the presence of solids; therefore, since the velocity profile and the cross-sectional area of the end of the sampling probe are known, the problem is reduced to controlling and measuring the aspiration rate.

4.5.2. Sampling System

Figure 4-8 illustrates the sampling system. The solids-gas sample is withdrawn continuously from the main stream through a sampling probe by means of a water aspirator. The sample flows through a Gelman filter holder (1 in. diameter, No. 1109) where the solids are collected. The magnitude of the air flow which leaves the filter, is controlled by a needle valve and indicated by a rotameter(Fisher and Porter Canada Limited, FP 1/4 - 25 - G - 5/81). A water manometer (Dwyer Mfg. Co., Michigan City

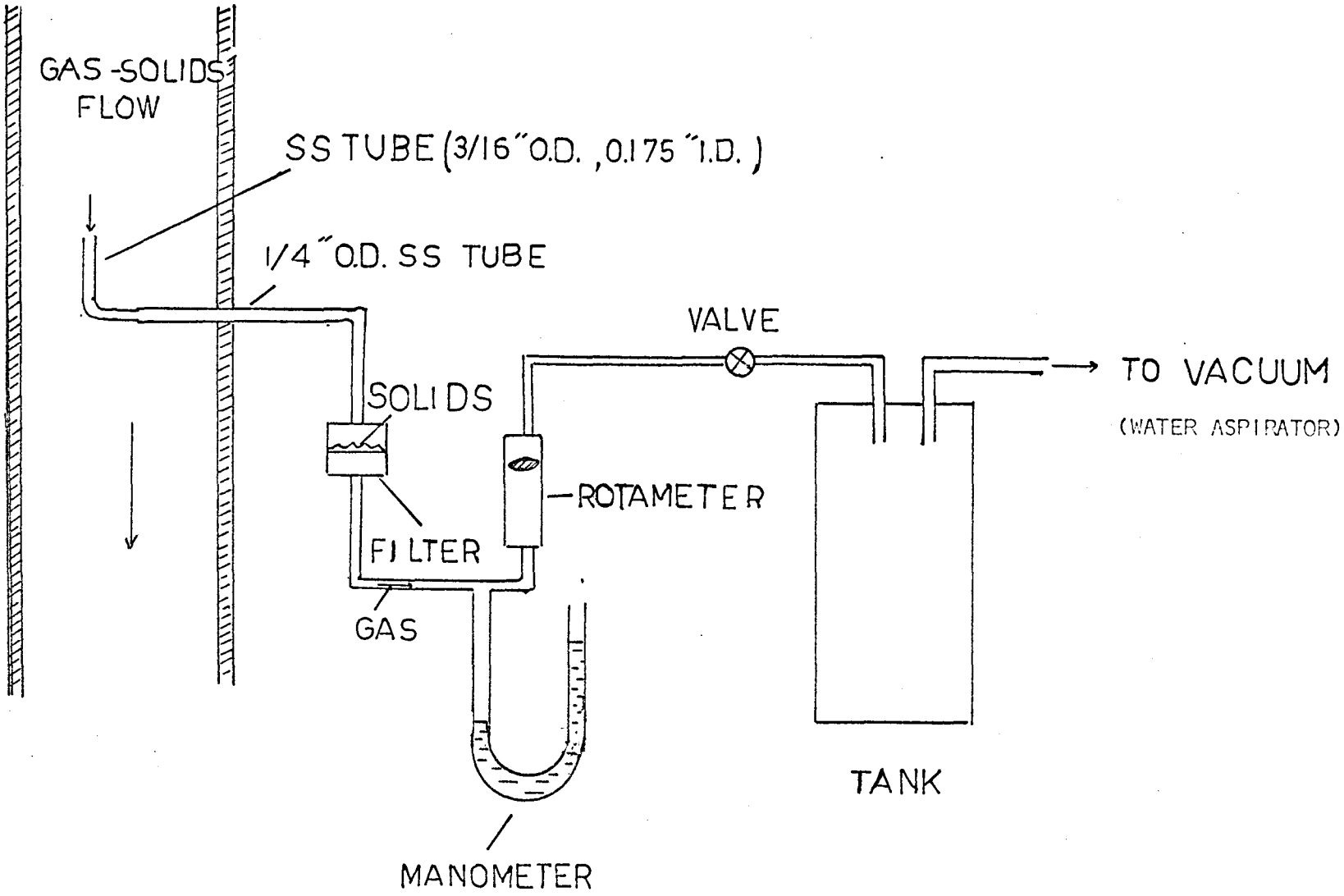

FIGURE 4-8 SCHEMATIC DIAGRAM OF SAMPLING SYSTEM

Ind.) located between the filter and the rotameter indicates the pressure drop of the gas stream. A glass tank of 0.4 cu.ft. in volume is installed between the control valve and the water aspirator in order to reduce the flow fluctuations. The ratio of the flow rate of solids over that of gas is a measure of particle concentration.

4.5.3. Sampling Probe and Traversing Mechanism

The sampling probe was made from a 3 in. length of 3/16 in. O.D. stainless steel tube inserted into a 1/4 in. O.D. stainless steel tubing so that the traversing mechanism (Figure 4-9) and the test position plug (Figure 4-10) designed by Koo can hold it at any desired radial position inside the pipe. The inside diameter at the inlet of the probe is 0.175 in. and was carefully smoothed both inside and outside.

Koo's traversing mechanism was slightly modified. As shown in Figure 4-9, it consists of a main semi-circular body, 3 in. long, with an inside diameter of 6 in. (outside diameter of the pipe). A 1 1/2 in. diameter hole was bored at the top of the main body in order to fit the protruding portion of the test position plug. The traversing mechanism was fixed to the pipe by the other half of the circular body of similar dimensions (not shown in Figure 4-9). A traversing plate passes through four parallel guiding rods fixed onto the main body. The traversing distance of the plate is measured by marks which were cut onto one of the guiding rods; these are 0.275 in. apart (equivalent to 1 tenth of the pipe inside

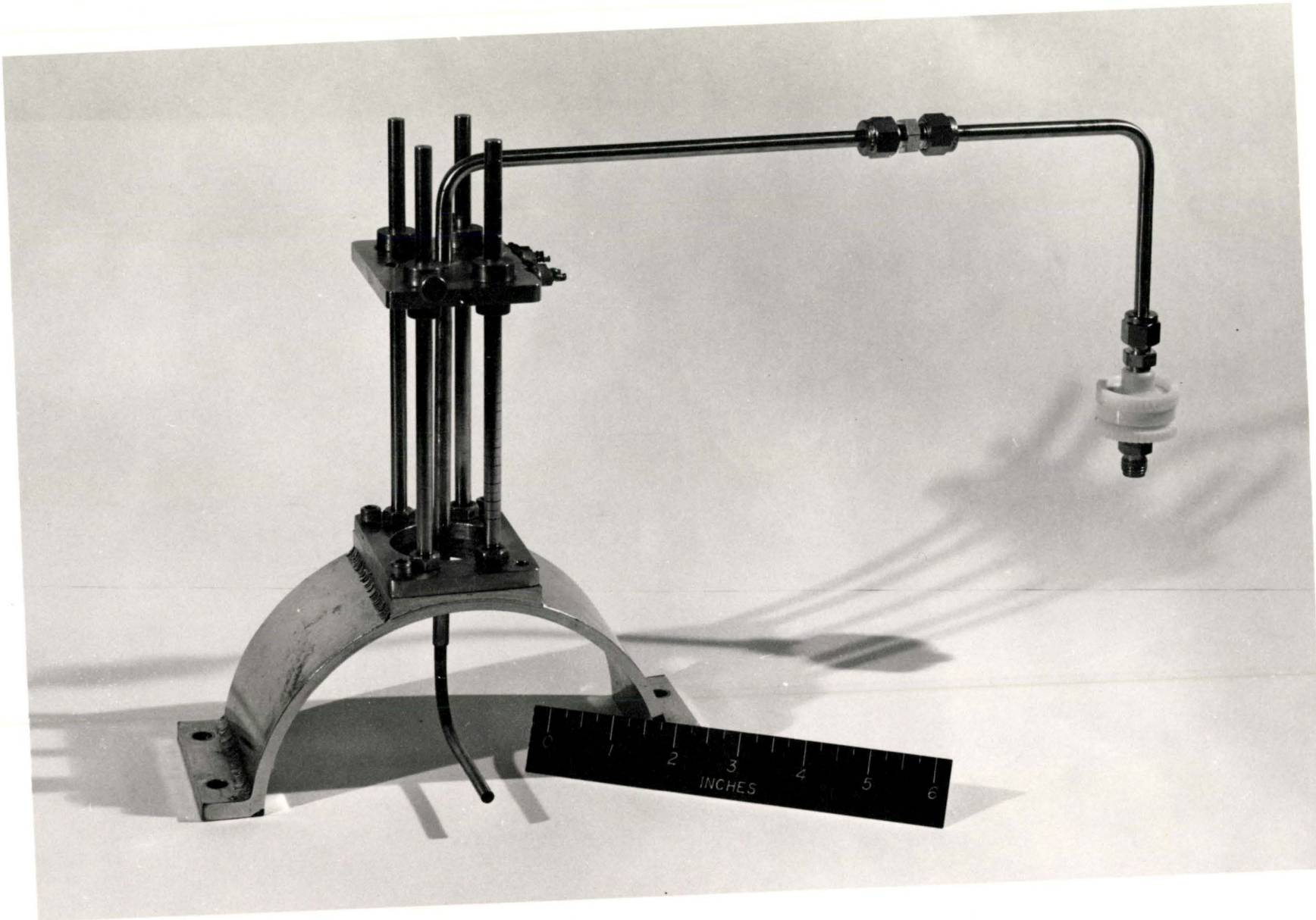

FIGURE 4-9 TRAVERSING MECHANISM

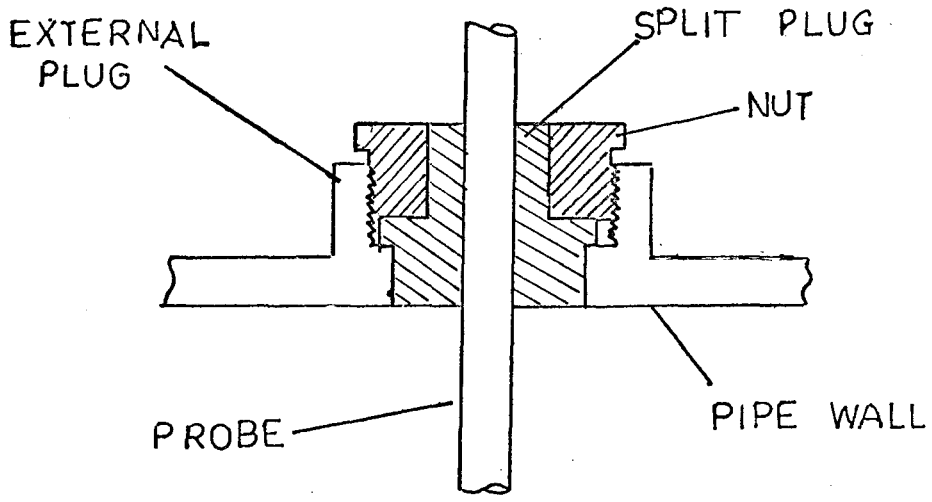

FIGURE 4-10 SAMPLING STATION SECTION

radius). The sampling probe passes through a 1/4 in. teflon O-ring located inside a 1/2 in. hole bored at the centre of the plate. It is fixed in position with respect to the plate by a set screw.

4.6 Gas-Solids Separation

The cyclone separator used in this work is a 2 1/2 Type Entrainement Separator (Wright-Austin Canada Limited). From their bulletin 810-D, the following information is taken:

Cyclone inlet diameter = 4 in.

Cyclone outlet diameter = 2 1/2 in.

Cyclone diameter by height: 7 3/4 in. by 14 in.

It is supposed to have a high efficiency for solids removed over a wide range of flow conditions. The separator has been stated to be capable of removing 99% of all solids entrainment where the particle size exceeds 10 microns.

The gas-solid flow section is reduced from 5.5 in. (pipe inside diameter) to 4 in. (cyclone inlet diameter) by a flanged connected steel pipe, 6 in. long. The solids discharge from the bottom of the cyclone into a 6 in. x 6 in. x 3 1/2 in. box which serves as a solids container. It is fixed outside the air box as shown in Figure 4-11 and this allows easy emptying at any convenient time. The weight of solids collected during a known time period (usually a run) is a measure of the solids-feed rate.

From the cyclone exit, the air passes through a glass fiber filter before it enters the fan where it is discharged into the room.

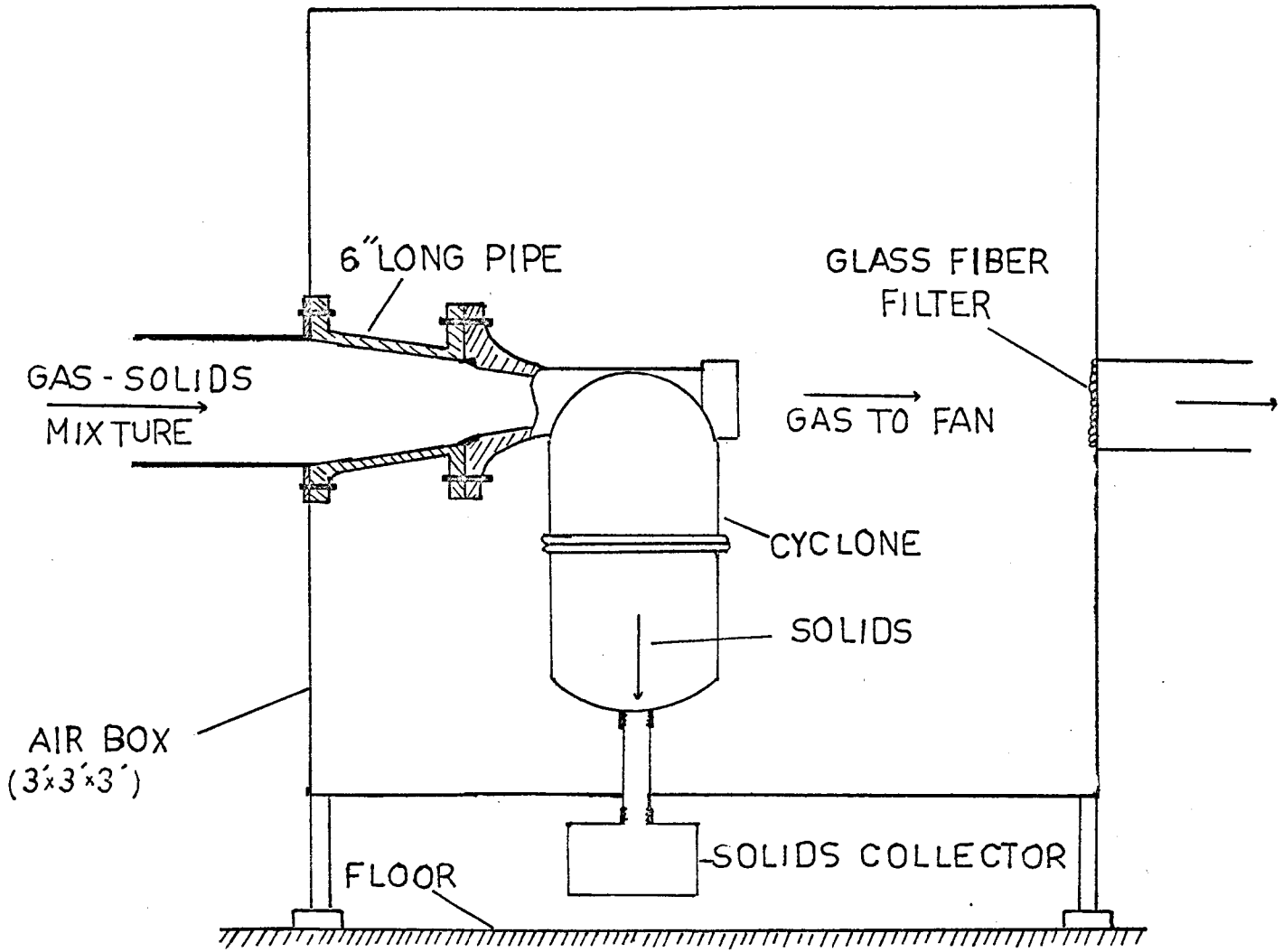

FIGURE 4-11 GAS-SOLIDS SEPARATION SYSTEM

4.7 Velocity Profile and Effects of Injector Location on Profile.

A velocity traverse was made at the test location by using a 1/4 in. O.D. Pitot tube and measuring the dynamic-to-static head difference on a water micromanometer (Model 34FB2TM, Merian Instrument Co., Cleveland, Ohio). The traversing mechanism described in section 4.5.3. was used to locate the Pitot tube inside the pipe; it allowed a vertical traverse only.

Unfortunately, it was found that the injector initially located in a vertical plane in the pipe had a considerable affect on the velocity profile downstream (the detailed measurements are given in section 5.1 and the results indicated on Figure 6-2). Since the particle sampling probe was to traverse over the same vertical section and since we wanted to avoid this asymmetric profile, it was decided to rotate the injection tube through 90^{o}. The velocity profile found under these conditions was symmetric (Figure 6-3); it has also agreed well with what is to be expected with fully-developed turbulent flow (Figure 6-4). It is expected in this case that the injector probe has little effect other than in the region immediately downstream of the probe.

5. EXPERIMENTS

5.1 Gas Velocity Measurement

Preliminary experiments were performed to measure the air velocity at the pipe axis versus fan speed. The Pitot-tube traverse yielded the velocity profile at a fan speed of 1100 r.p.m. This high speed was chosen in order to reduce as much as possible the effect of gravity on glass beads. Although the solids were not fed during these velocity traverses, all equipment for their injection was in place.

Because the concentration of solid particles was very small, no effect on the velocity profile is expected. Therefore, all the experimental results on particle diffusion correspond to this gas flow. The curve relating centre-line velocity to motor speed was used to allow ease in setting up other experimental conditions and to evaluate changes in air velocity that might occur with small changes in motor speed during the course of a run.

In all runs reported here, the injector tube was located in the horizontal plane for the reasons mentioned in section 4.7.

5.2 Particle Concentration Measurement

5.2.1. Procedure

Before beginning a run, the solids were filled to a height of 9 in. in the upper tank and 6 in. in the lower tank of the solids feeder. The solids collector was fixed to the bottom of the cyclone. The fan motor was turned on and the motor speed was adjusted at 1100 r.p.m. using a tachometer. It was found that if the motor speed was controlled

frequently, the air flow reached steady-state about 30 minutes after the motor start-up; this was tested by observing the pressure drop of the air flowing in the pipe.

As soon as the steady air flow was established, the solids feeder was turned on, following the steps below:

The air which transported the solids into the pipe, was controlled to yield the isokinetic rate, i.e., the air velocity at the outlet of the particle injector was equal to the velocity at the pipe axis of the main flow. The rotary solids-feeder was turned on. The auxiliary air flow was fed at a rate of about 0.008 cu.ft./min. into the lower tank. The vibrator was turned on with a voltage setting of 90 volts and at the same time, a timer was started. The timer was used to measure the total time during which the solids were fed into the system.

During the first 15 minutes of experiment, the rotary-valve speed was adjusted to keep the solids level in the lower tank as constant as possible. After this initial period, it was found that this speed needed to be adjusted slightly every 15 minutes in order to keep the variation of solids level within a range of $\pm$ 0.15 in.

Once the solids feeder was functioning smoothly, solid concentrations were obtained using the traversing mechanism and the isokinetic sampling system described previously. Before starting the runs, small glass containers (1 in. high, 1 1/4 in. diameter) containing a filter paper were weighed and properly identified with a particular position. All weights were determined on a Fisher Scientific Microbalance (measurement to $\pm$ 0.5 mg). At each radial position, a filter paper was inserted in the holder and the flowrate was set to ensure isokinetic sampling.

The exact location of the sampling probe was set with the aid of a magnifying glass on the graduated scale of the sampling traversing mechanism. When everything was in position, the appropriate valve was opened to start the sampling; fine adjustments to air flow were made to attain the correct sampling rate. The sampling time was determined by a stop-watch. Normally the proper conditions could be obtained within about 30 seconds; the sampling time was usually about 2 to 7 minutes depending upon solid concentration at injection, and axial and radial position. At the end of sampling time, the air was turned off and the filter paper along with solids were reweighed in the original container.

When the run was completed, the solids feeder and the timer were stopped at the same time. The fan motor was shut off; the solids collected in the solids collector were discharged and weighed in order to determine the solids-feed rate. As the latter remained quite constant during a single run of approximately 2 hours, only one concentration profile was measured during the run.

5.2.2. Sampling Difficulties

One of the difficulties during sampling was manifested by the fluctuation of the rotameter float due to the presence of solids in the gas flow. Because of this, the sampling flow-rate required continual attention to keep it constant.

A second difficulty arose when the filter paper was not perfectly flat or not well located in the holder. This allowed solids to get through to the rotameter. This condition could be easily detected by the manometer at the filter, since normally it indicated a 12 to 22 in. water

vacuum, but in those cases with poor filtration, the manometer registered only about 6 in. water vacuum.

Finally it was found that if the filter contained more than 0.20g of solids, considerable difficulty was experienced in transferring filter plus solids into the container without losing some of the beads.

6. EXPERIMENTAL RESULTS

6.1 Gas Velocity

The data presented in this paragraph was evaluated at flow conditions of 1 atm. and 77°F. (average temperature during the experiments). Detailed calculations are given in Appendix A.1.

The relation between the air velocity at the pipe axis versus the fan speed is shown in Figure 6-1. The effects of injector location on velocity profile are presented in Figures 6-2 and 6-3. The experiments were carried out at a Reynolds number of 52800 which was based on mass flow calculated from the symmetrical profile (Figure 6-3). The latter was converted in dimensionless form u^+ versus y^+ in order to be compared with Koo's data at Re = 58300 and with Deissler's semi-empirical equation (9) as shown in Figure 6-4. The results indicate that the maximum deviation between the present data and Deissler's equation is only 3.5%.

6.2 Particle Concentration Profile

The particle concentration profiles at Re = 52800 were measured under different rates of solids flow. They are presented in dimensionless form M/M_∞ in Figures 6-5 to 6-8 for which M_∞, the completely mixed concentration was determined from the ratio of the solids-feed rate over the air flow rate. These mass profiles of particles are unsymmetrical about the pipe axis because of the gravity of the particles. This effect reduced the range of studies. Data were obtained at only 4 different downstream positions, nominally, 18, 30, 42 and 54 in. from the injector mouth. Each profile was formed by 10 to 11 radial positions.

The maximum solids flow-rate was 5g/min which corresponds to a solids-gas loading W_p/W of 0.008. The above choice was governed by sampling difficulties discussed previously.

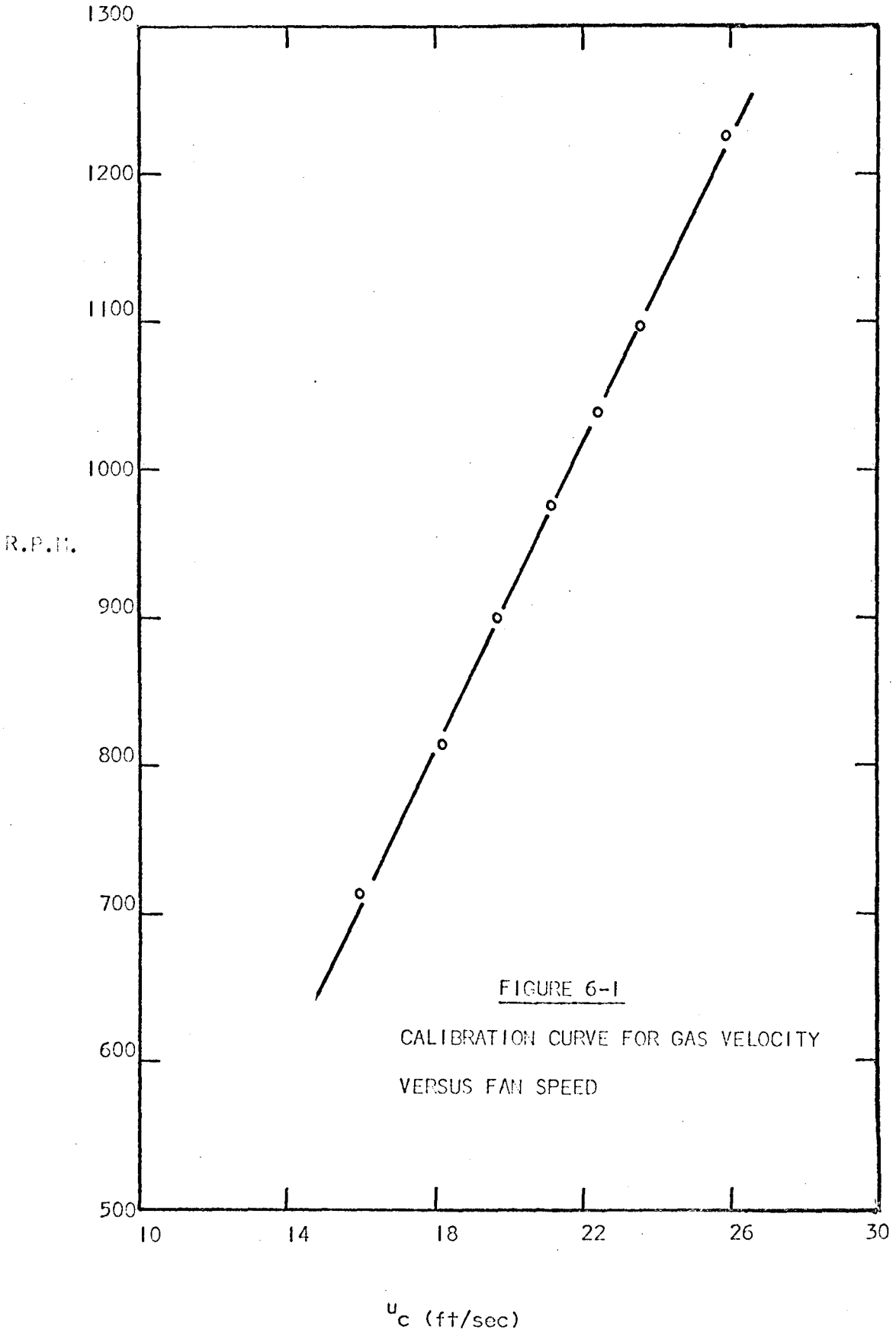

FIGURE 6-1

CALIBRATION CURVE FOR GAS VELOCITY VERSUS FAN SPEED

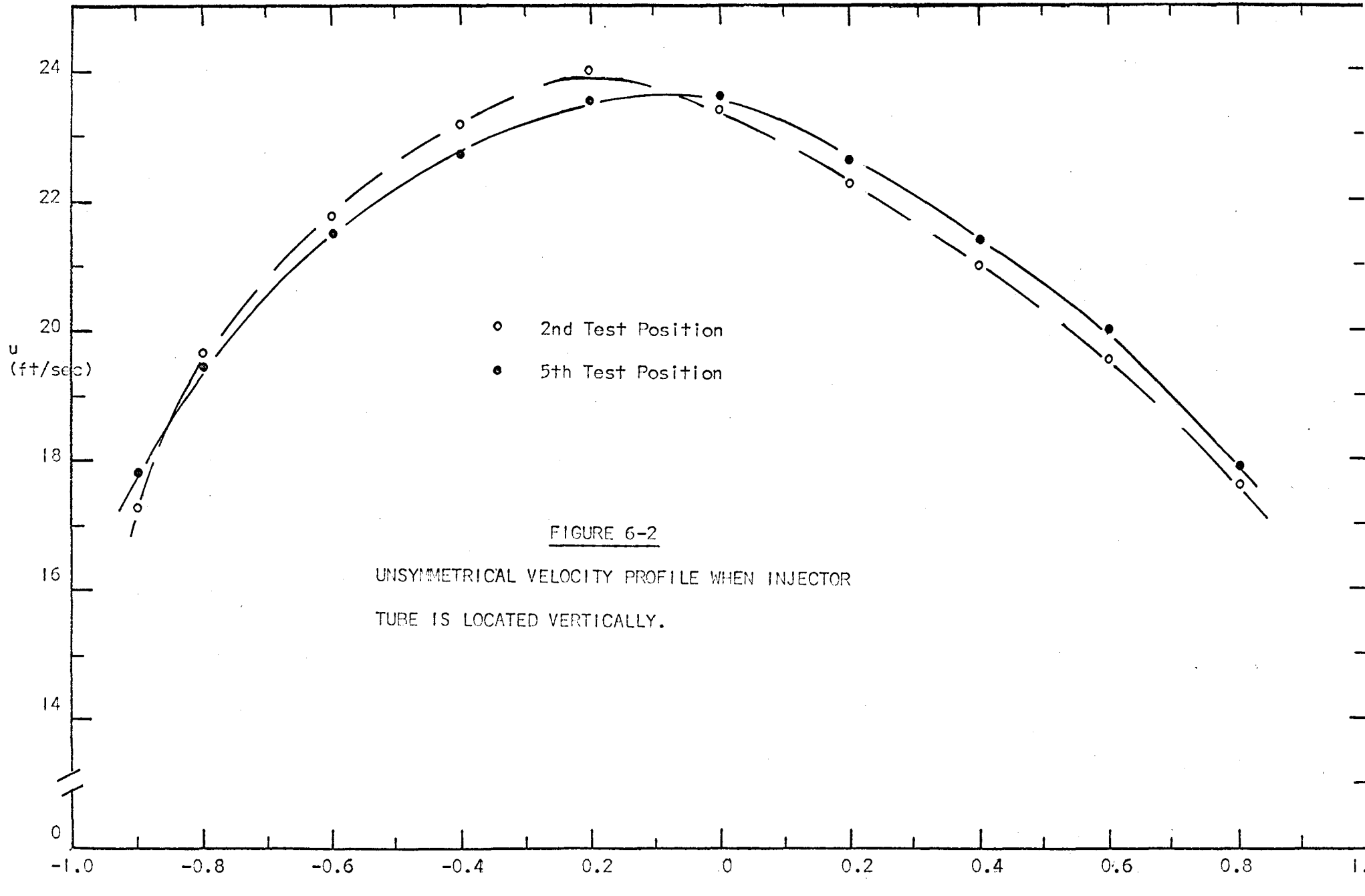

FIGURE 6-2

UNSYMMETRICAL VELOCITY PROFILE WHEN INJECTOR TUBE IS LOCATED VERTICALLY.

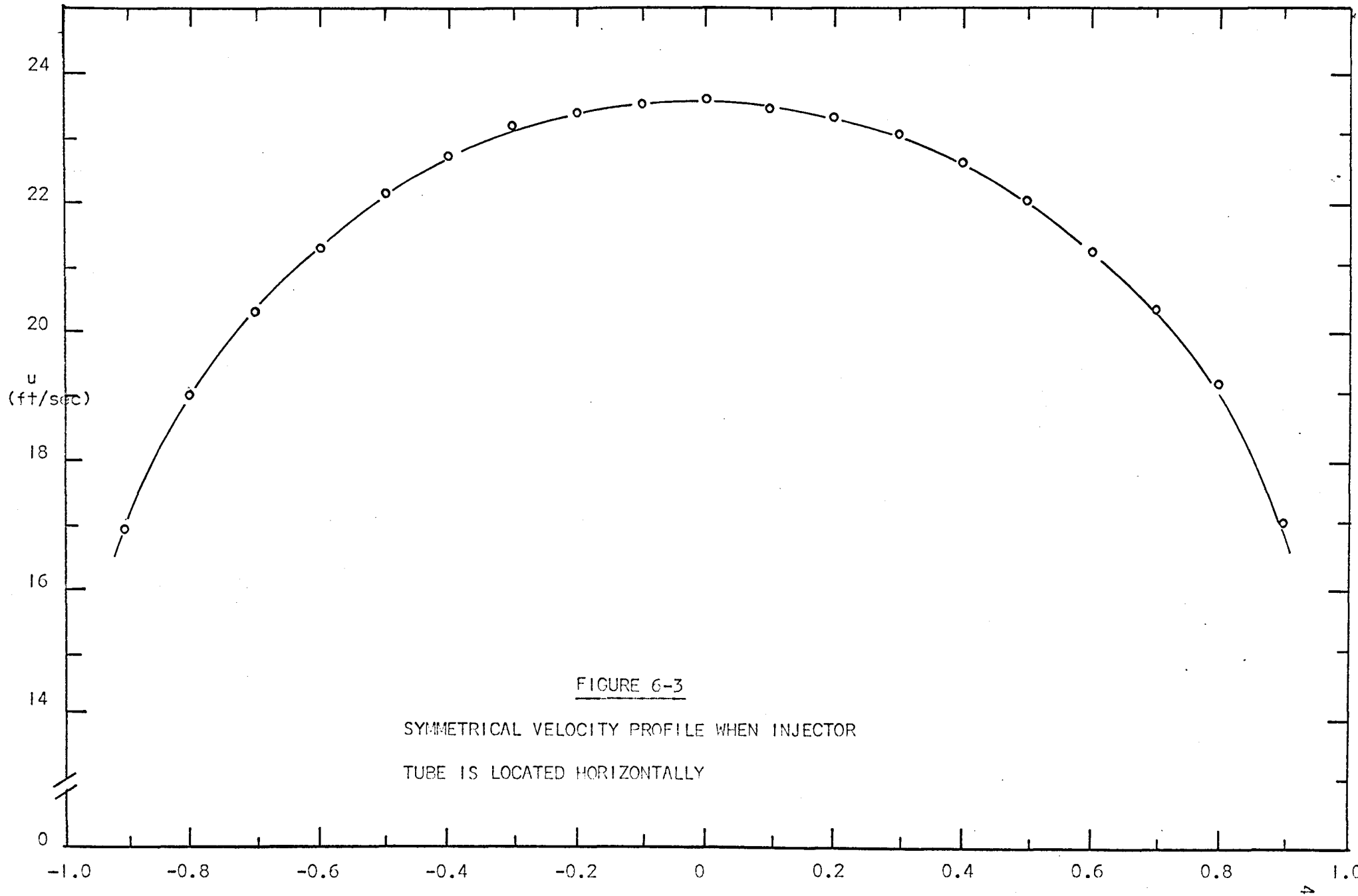

FIGURE 6-3

SYMMETRICAL VELOCITY PROFILE WHEN INJECTOR TUBE IS LOCATED HORIZONTALLY

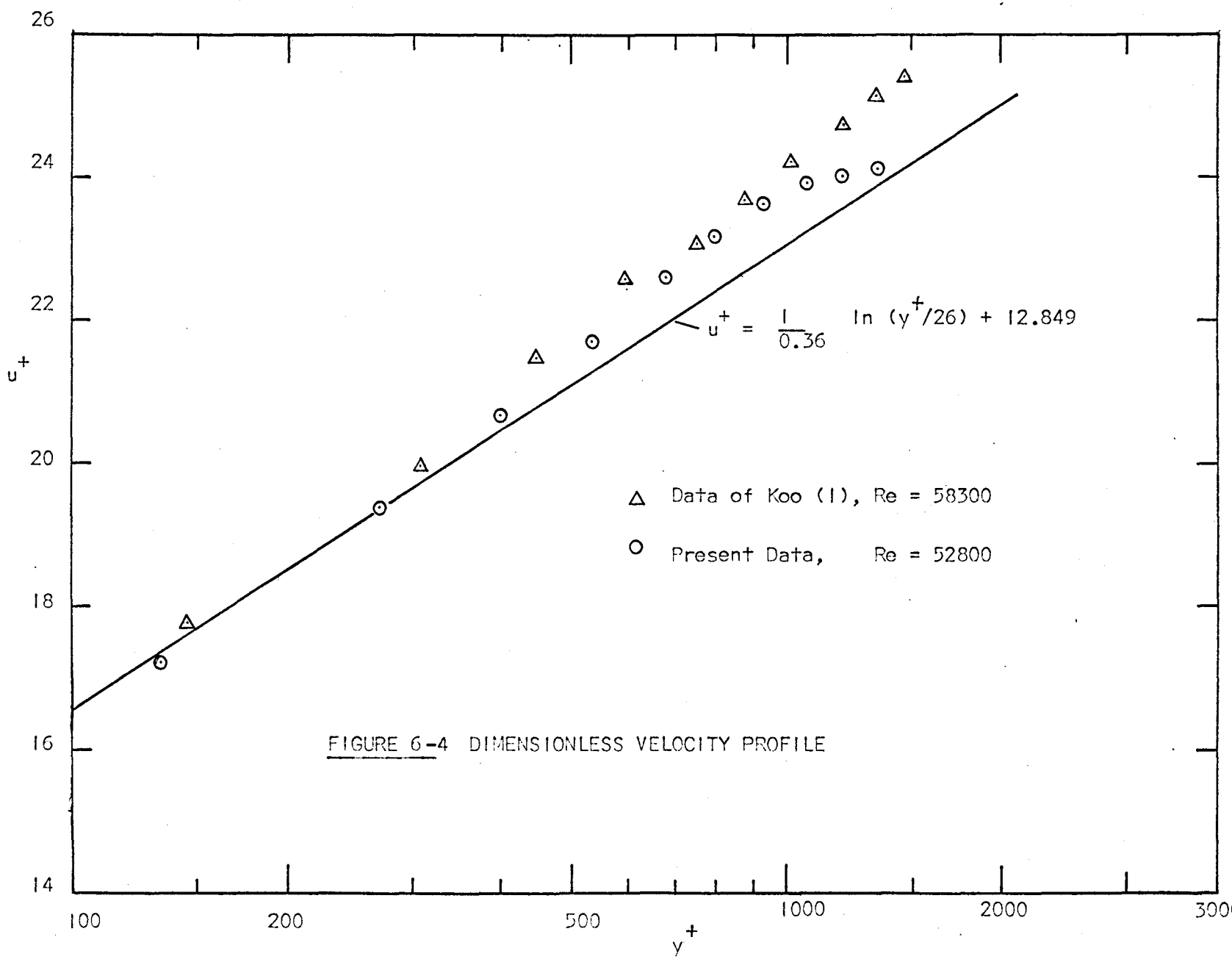

FIGURE 6-4 DIMENSIONLESS VELOCITY PROFILE

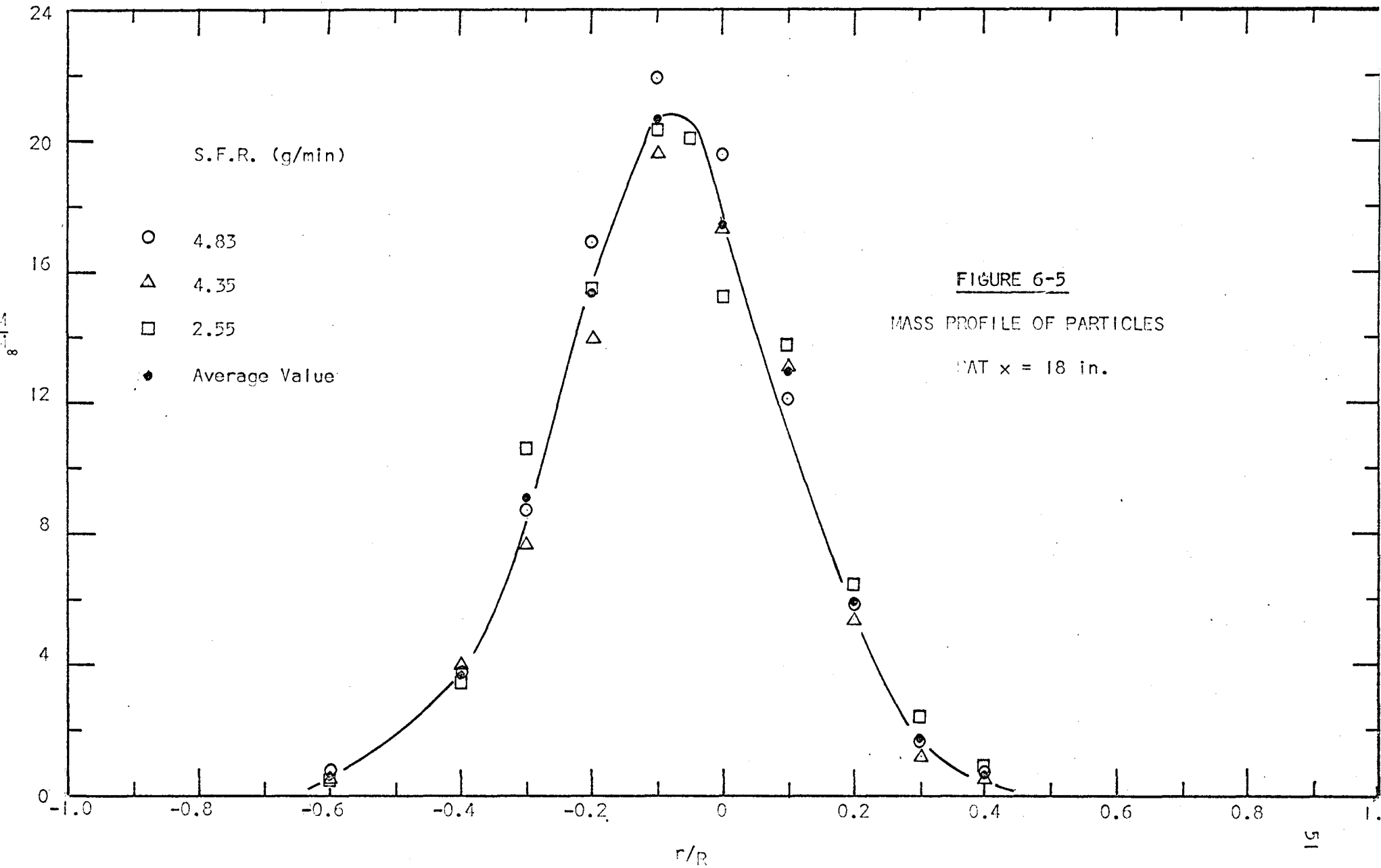

FIGURE 6-5

MASS PROFILE OF PARTICLES

AT x = 18 in.

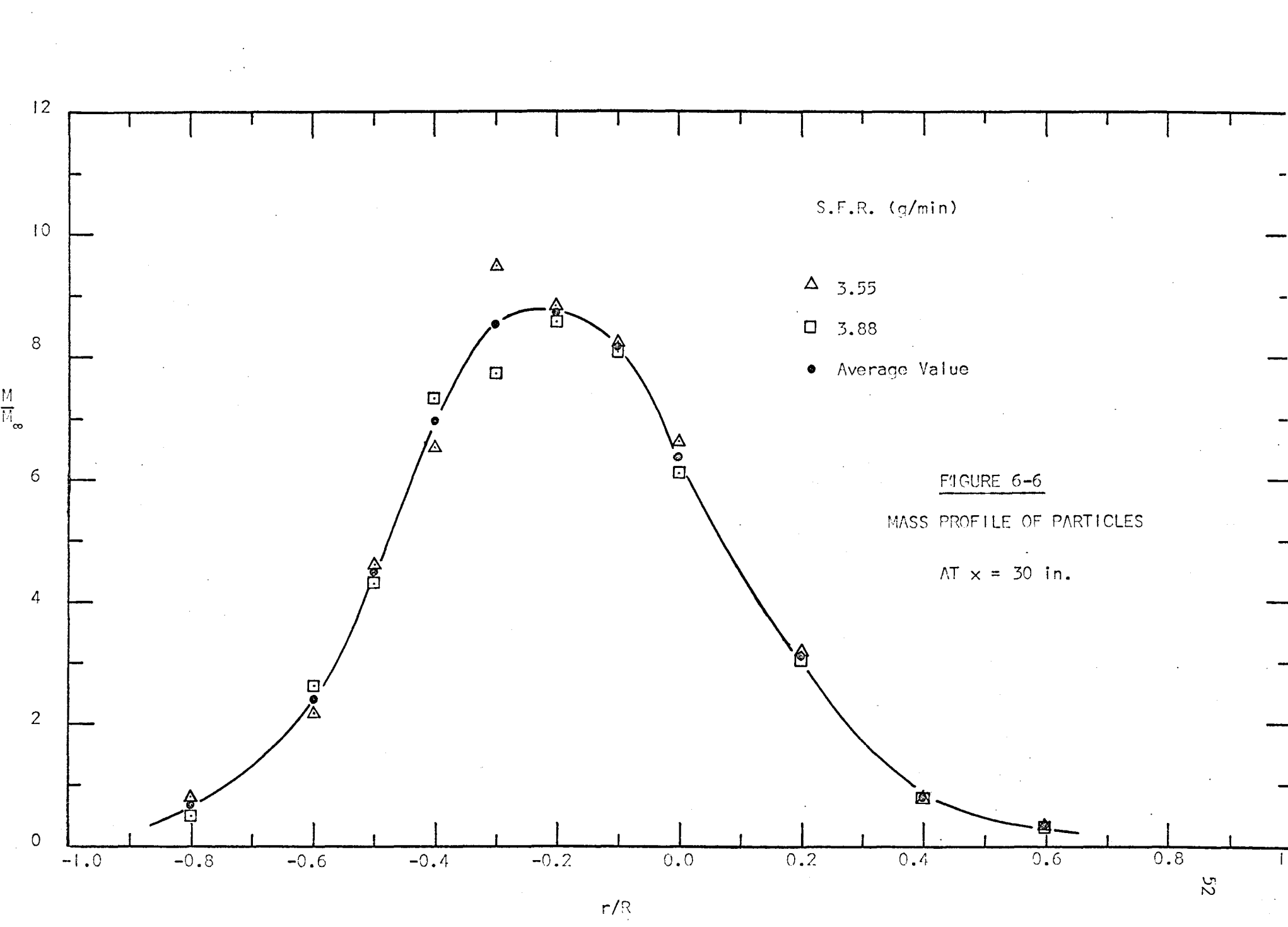

FIGURE 6-6

MASS PROFILE OF PARTICLES

AT x = 30 in.

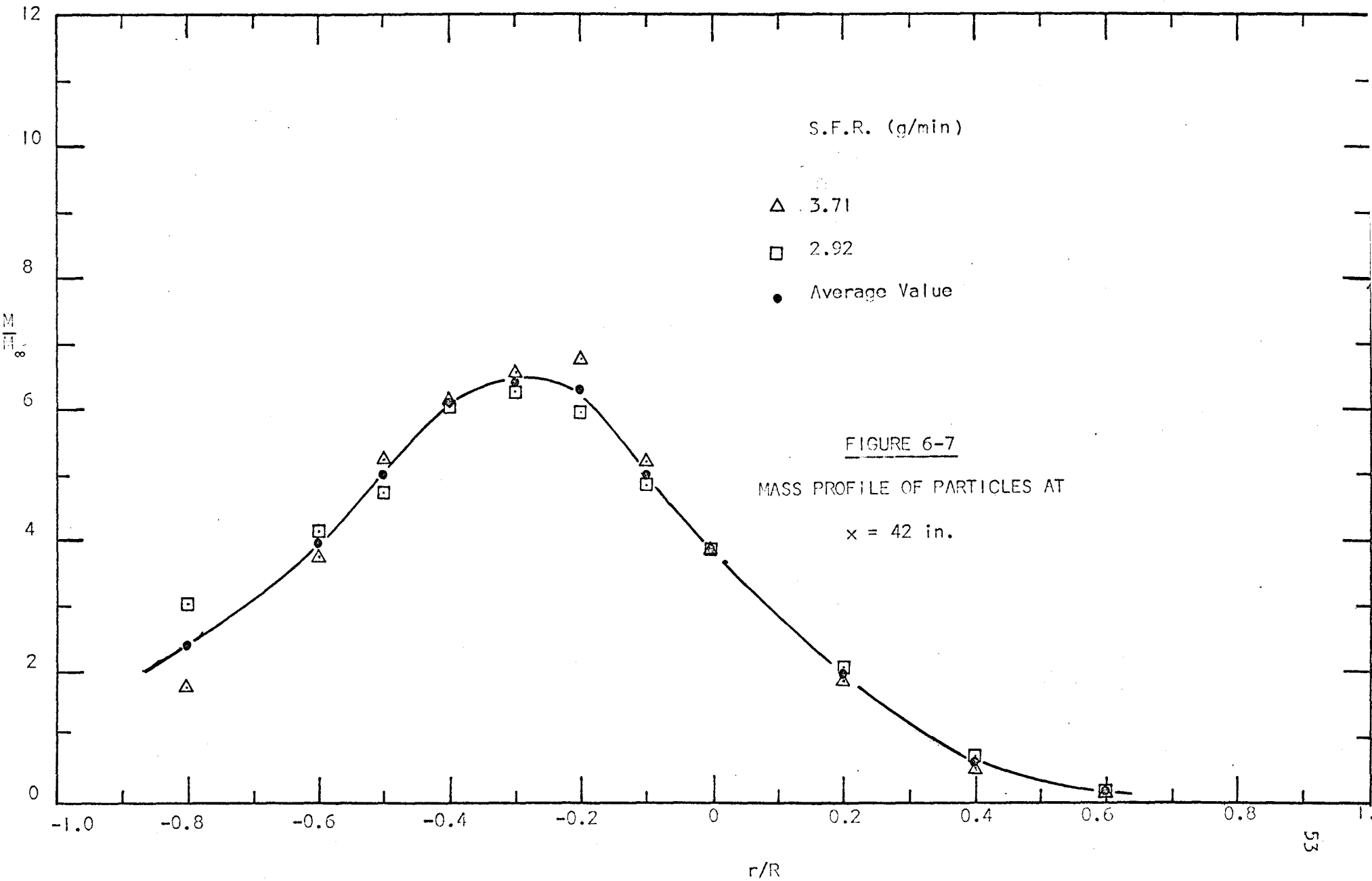
S.F.R. (g/min)
△ 3.71
□ 2.92
● Average Value
FIGURE 6-7
MASS PROFILE OF PARTICLES AT
x = 42 in.
12
10
8
6
4
2
0
-1.0
-0.8
-0.6
-0.4
-0.2
0
0.2
0.4
0.6
0.8
r/R

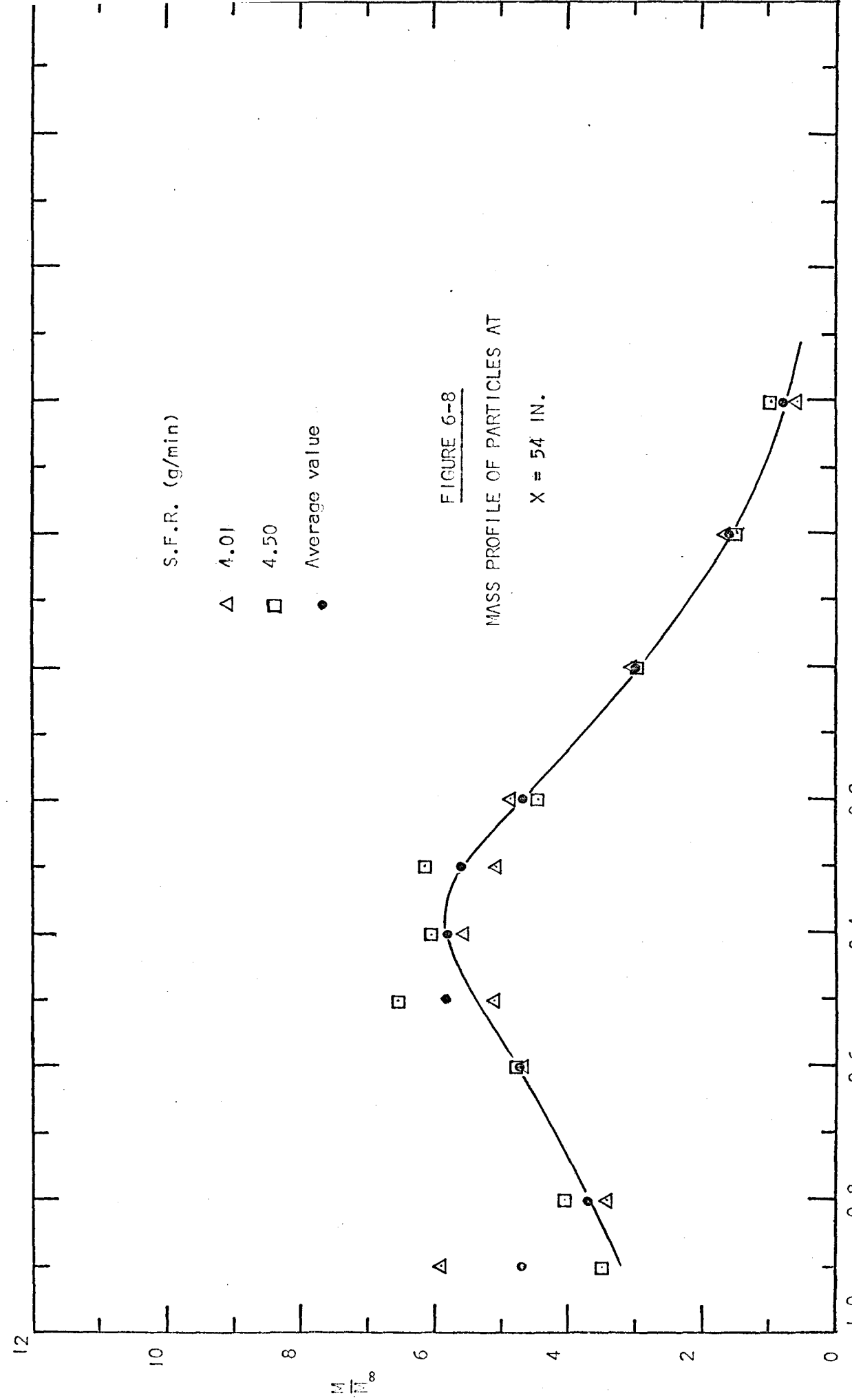

FIGURE 6-8

MASS PROFILE OF PARTICLES AT X = 54 IN.

7. TREATMENT OF DATA AND RESULTS

This chapter is concerned with the determination of the eddy diffusivity ε_p of the particles from the experimental values of $M(r)/M_\infty$ This coefficient may or may not change appreciably with particle size. Therefore, two separate cases were considered; one on the assumption that ε_p is a constant, the other based on an assumed functional relationship of ε_p with particle size.

7.1 Governing Equations and Assumptions

In Chapter 3, it was shown that if the eddy diffusivity and the average velocity were constant over the entire flow section, then the concentration of particles at any radial and axial position could be obtained from:

$$\frac{C}{C_\infty} = 1 + \frac{2R}{b} \sum_{n=1}^{\infty} \frac{J_1\left(\beta_n \frac{b}{R}\right) J_o\left(\beta_n \frac{r}{R}\right) \exp\left(-\beta_n \varepsilon_p \times / UR^2\right)}{\beta_n J_o^2(\beta_n)} \qquad (3\text{-}28)$$

This equation is presented graphically by the solid lines in Figure 7-3; Appendix A.2 indicates the details of the computer program used to generate the data for Figure 7-3.

However, the experimental data $M(r)/M_\infty$ must be transformed to $C(r)/C_\infty$ and a correction for the effect of gravity on the particles must be included.

$M(r)/M_\infty$ is expected to be different from $C(r)/C_\infty$ if the particles are not of uniform size. If the particles are polydispersed then gravity will

cause some separation and also the turbulent eddies are expected to move the smaller particles more efficiently. The result is that the particle size distribution at each sampling point may be different from that in the original tracer.

This can be most easily demonstrated by expressing M in terms of C :

$$M = C \left[\left(\frac{\pi d_v^3}{6} \right) \rho_p \right] \tag{7-1a}$$

The term in the square bracket represents the mass of a single particle of size d_v and d_v is the volume average diameter, given by:

$$d_v = \left[\frac{\Sigma n_i \, d_i^3}{\Sigma n_i} \right]^{1/3} \tag{7-2}$$

An expression similar to (7-1a) may be written for M_∞:

$$M_\infty = C_\infty \left[\left(\frac{\pi d_{v\infty}^3}{6} \right) \rho_p \right] \tag{7-1b}$$

Hence

$$\frac{M}{M_\infty} = \frac{C}{C_\infty} \left(\frac{d_v}{d_{v\infty}} \right)^3 \tag{7-3a}$$

or

$$\frac{C}{C_\infty} = \frac{M}{M_\infty} \left(\frac{d_{v\infty}}{d_v} \right)^3 \tag{7-3b}$$

In order to make a correction for gravity, the following assumptions were made:

(1) The velocity and turbulent parameters of gas are constant in the central core.

(2) The particle velocity and gas velocity in the axial direction are equal.

(3) The relative motion of the particle to the fluid is given by Stokes's law.

The validity of these assumptions will be discussed in section 8.2.

The fall velocity of a particle of mass m as a function of time can be determined by solving the following equation of motion:

$$m \frac{dv_p}{dt} = mg (\rho_p - \rho) - F_D \qquad (7\text{-}4)$$

which represents a balance between the force required to accelerate the particle, the gravitational force and the drag force.

By definition:

$$F_D = \frac{C_D v_p A_p}{2} \qquad (7\text{-}5)$$

where $A_p = \pi d^2/4$ is the cross-sectional area of the particle.

From assumption (3), the drag coefficient, C_D, is:

$$C_D = \frac{24}{Re_p} \qquad (7\text{-}6)$$

where Re_p, Reynolds number, for falling spheres, is given by:

$$Re_p = \frac{dv_p \rho}{\mu} \qquad (7\text{-}7)$$

Substituting equations (7-5) and (7-6) into equation (7-4) yields:

$$\frac{dv_p}{dt} = - \left(\frac{18\mu}{d^2 \rho_p} \right) v_p + \frac{g(\rho_p - \rho)}{\rho_p} \qquad (7\text{-}8)$$

With the initial condition $v_p = 0$ at $t = 0$, the solution of the differential equation (7-8) is:

$$v_p = v_t \left[1 - \exp (-kt) \right] \tag{7-9}$$

where

$$k = \frac{18\mu}{d^2 \rho_p} \tag{7-10a}$$

and

$$v_t = \frac{g(\rho_p - \rho)d^2}{18\mu} \tag{7-10b}$$

v_t is the terminal velocity of the particle.

The distance from centre line that the particle falls at a given time, t, since its injection into the pipe, can be obtained by integrating equation (7-9):

$$\ell = \int_0^t v_t \left[1 - \exp (- kt) \right] \, dt \tag{7-11}$$

or

$$\ell = v_t t - \frac{v_t}{k} \left[1 - \exp (- kt) \right] \tag{7-12}$$

From assumptions (1) and (2), the time necessary for the particle to move from the tracer injector to an axial position x is:

$$t = \frac{x}{u_c} \tag{7-13}$$

Thus the dimensionless distance, ℓ/R, becomes:

$$\frac{\ell}{R} = \frac{v_t}{R}\left(\frac{x}{u_c}\right) - \frac{v_t}{RK}\left[1 - \exp\left(-k\frac{x}{u_c}\right)\right] \qquad (7\text{-}14)$$

Since v_t is proportional to d^2, the correction for gravity should be made for each group of particles of narrow size. This is the principle of the methods developed below:

7.2 Calculations Assuming Particle Diffusivity is independent of Particle Size.

Let us consider first the case in which the coefficient ε_p is assumed constant for all particles.

The determination of ε_p could be made in two ways: The first consists of transforming the unsymmetrical profile M/M_∞ to symmetrical profile C/C_∞ by using experimental values of d_v, correcting for gravity and then using equation (3-28) to calculate ε_p to fit the data. The second is the inverse; a constant value of ε_p is assumed and a radial profile C/C_∞ is calculated, gravity is included and the profile of M/M_∞ is obtained and compared with the actual experimental measurements.

It should be noted that the effects of an asymmetric distribution of particles are not considered in any method. Since the gas velocity and turbulent parameters are relatively constant over the central core, this effect may not be of primary importance. As the particles migrate into the wall region, there is no doubt that there will be an effect; therefore, more weight should be given to the experimental data in the central core.

7.2.1. Method 1

7.2.1-1 General Outline of the Method

The calculation procedure adopted to transform the mass profile to a correct concentration profile is composed by the following steps:

(a) Transformation of M/M_∞ to C/C_∞

The experimental values of M/M_∞ were first converted to C/C_∞ using equation (7-3b) and the experimentally measured particle size distributions of the samples and that of the original tracer.

(b) Decomposition of Concentration to its Component Parts According to Particle Size

Each C/C_∞ was then decomposed to a sum of C_i/C_∞ where:

$$C_i = C \cdot f(d_i), \quad i = 1, 2, \ldots, m$$

$f(d_i)$ = fraction of particles of size d_i in a sample (experimental value)

m = number of size groups chosen to represent the distribution.

(c) Correction for gravity

Using equation (7-14), a correction for gravity was applied to each size group at each of the radial positions where the measurements were made. This allowed a plot of the concentration profile to be made for each size group as shown in Figure 7-1. At any radial position, the concentrations of all particles were added to give a total concentration, radial profile as shown in Figure 7-2 by the full line curve.

(d) Normalization

Assuming a uniform velocity field, as in equation (3-28), a population balance on the particles requires that:

$$2\int_0^R \pi C r dr = \pi R^2 C_\infty \qquad (7\text{-}15a)$$

where C_∞ is the concentration of the particles when they are uniformly dispersed throughout the gas stream. This equation may be rearranged to give:

$$2\int_0^1 \left(\frac{C}{C_\infty}\right) z dz = 1 \qquad (7\text{-}15b)$$

where $z = r/R$

The completely mixed concentration C_∞ as mentioned previously can be obtained from the air flow rate measurement and the weight of the solids collected from the cyclone over a run.

Since the value of C depends on sampling error and measurements of particle-size distribution, and C_∞ is a completely independent measurement, the balance depicted by equation (7-15a) or (7-15b) is an indication of the accuracy of these measurements. On the other hand, the use of equation (3-28) is based on the population balance being maintained; therefore each experimental measurement is adjusted or normalized by:

$$\left(\frac{C(z)}{C_\infty}\right)_n = \frac{\frac{C(z)}{C_\infty}}{2\int_0^1 \frac{C(z)}{C_\infty} z dz} \qquad (7\text{-}16)$$

where the subscript n indicates the normalized values.

This procedure assumes the same percentage error with each point.

(e) Calculation of the Eddy Diffusivity.

The calculation of $\varepsilon_p x/UR^2$ or ε_p follows directly from Figure 7-3 once the correct profile C/C_∞ at any traverse position x is known.

As ε_p and u are assumed constant over the pipe diameter, the experimental values of C/C_∞ at various radial positions r/R must lie on a vertical line which corresponds to a constant value of $\varepsilon_p x/UR^2$ as shown in the Figure.

7.3.1-2. Detailed Calculations from Experimental Data

This method is illustrated by treating the experimental data for the profile at x = 18 in.

Particle size distributions of 10 samples were measured experimentally. Six size groups were used, each comprising 10 micron spread. The average diameters, d_i, are 5, 15, 25, 35, 45 and 55 microns respectively.

The data for M/M_∞, d_v, C/C_∞ and $f(d_i)$ at different radial positions are shown in Table 7-1. The results for ℓ/r are included in Table 7-2. Figure 7-1 presents the profiles C_i/C_∞ after correcting for gravity using values in Tables 7-1 and 7-2. The solid line in Figure 7-2 is the unnormalised curve C/C_∞ which passes through the average values of two points located at the opposite side of the centre line. That is, the profile was made symmetrical by this averaging procedure. The non-symmetry at several points of the total profile is due mainly by the linear interpolation of profiles C_i/C_∞ in Figure 7-1.

TABLE 7-1

DATA FOR M/M_∞, C/C_∞ AND $f(d_i)$ AT X = 18 in.

$\frac{r}{R}$	$\frac{M}{M_\infty}$	$d_v(\mu)$	$\frac{C}{C_\infty}$	f(5μ)	f(15μ)	f(25μ)	f(35μ)	f(45μ)	f(55μ)
-0.6	0.56	43.5	0.30	.001	.016	.101	.283	.360	.160
-0.4	3.75	39.6	2.65	.003	.037	.195	.370	.295	.100
-0.3	9.00	38.9	6.68	.004	.048	.213	.380	.270	.085
-0.2	15.45	34.3	17.1	.010	.090	.320	.385	.175	.030
-0.1	20.60	35.8	20.2	.003	.050	.257	.430	.224	.036
0.0	17.35	35.0	19.2	.003	.062	.310	.435	.171	.019
0.1	12.98	37.5	10.9	.004	.051	.240	.395	.250	.060
0.2	5.87	35.5	5.85	.008	.074	.278	.380	.215	.045
0.3	1.78	38.6	1.36	.012	.078	.235	.345	.240	.090
0.4	0.62	35.8	0.60	.015	.085	.250	.350	.220	.090

The denominator of equation (7-16) was found to be 1.20 by integrating the solid line, that is, the difference between the normalized and unnormalized curves is 20%.

Figure 7-3 shows that the best agreement between the normalized data and equation (3-28) was obtained by taking $\varepsilon_p x/UR^2$ equal to 0.0145. This agreement can be easily determined by an iterative procedure. The particle diffusivity at x = 18 in. was then calculated to be:

TABLE 7-2

VALUES OF ℓ/R^* VERSUS PARTICLE SIZE

AND AXIAL DISTANCE

d_i (μ) \ x(in)	18	30	42	54
5	.002	.003	.004	.005
15	.011	.020	.027	.035
25	.038	.066	.095	.123
35	.070	.127	.182	.236
45	.014	.195	.288	.383
55	.139	.270	.405	.543

* Detailed calculations are given in Appendix A.3.

$$\frac{\varepsilon_p}{UR} = 22.2 \times 10^{-4}$$

and

$$\varepsilon_p = 9.7 \times 10^{-3} \text{ ft}^2/\text{sec}$$

(Note U = 19.2 ft/sec, see Appendix A.1)

Although this method was applied successfully for the data at x = 18 in., it did not give any result for three remaining data. The main reason is that for the data at x = 18 in., the particle size distribution of each of the ten samples located in the range of r/R = -0.6 to + 0.4 were measured; in the other cases, they were measured at only six to seven samples at positions in a wider range of r/R (r/R = -0.8 to

FIGURE 7-1 CONCENTRATION PROFILES AT x = 18 in. FOR DIFFERENT SIZE GROUPS AFTER CORRECTING FOR GRAVITY.

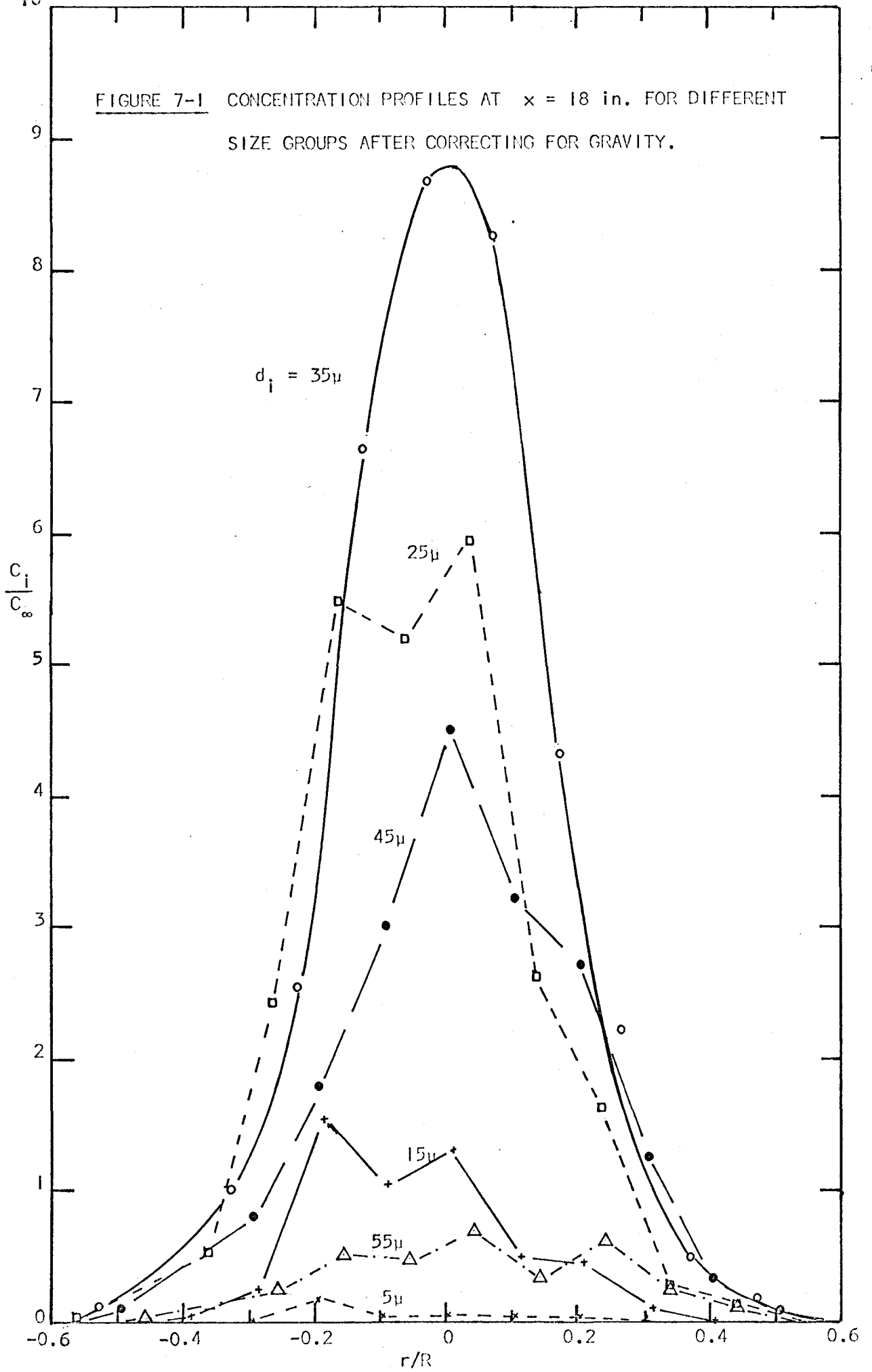

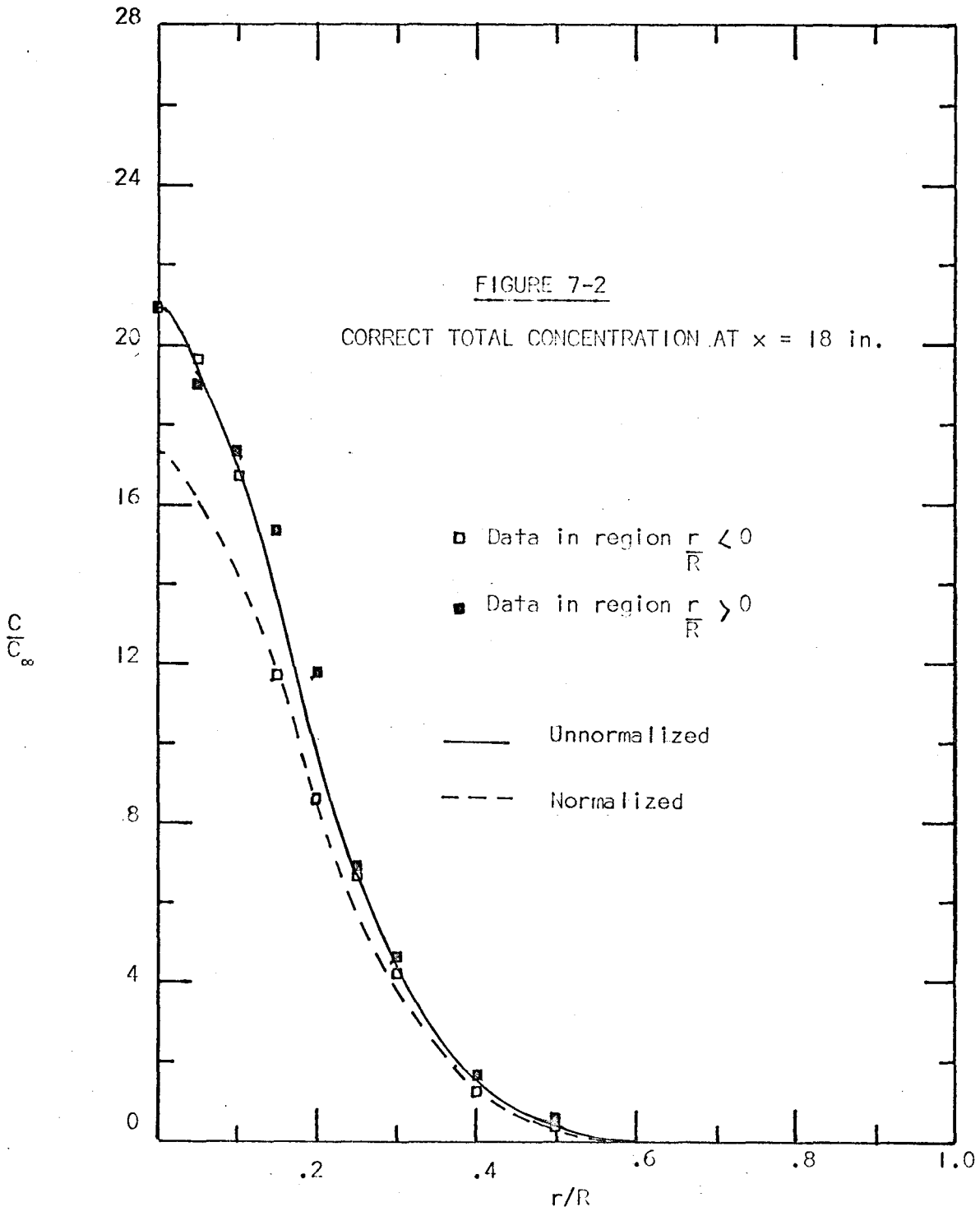

FIGURE 7-2

CORRECT TOTAL CONCENTRATION AT x = 18 in.

FIGURE 7-3

GRAPHICAL PRESENTATION OF THEORETICAL EQUATION (3-28)

AND COMPARISON WITH DATA AT x = 18 in.

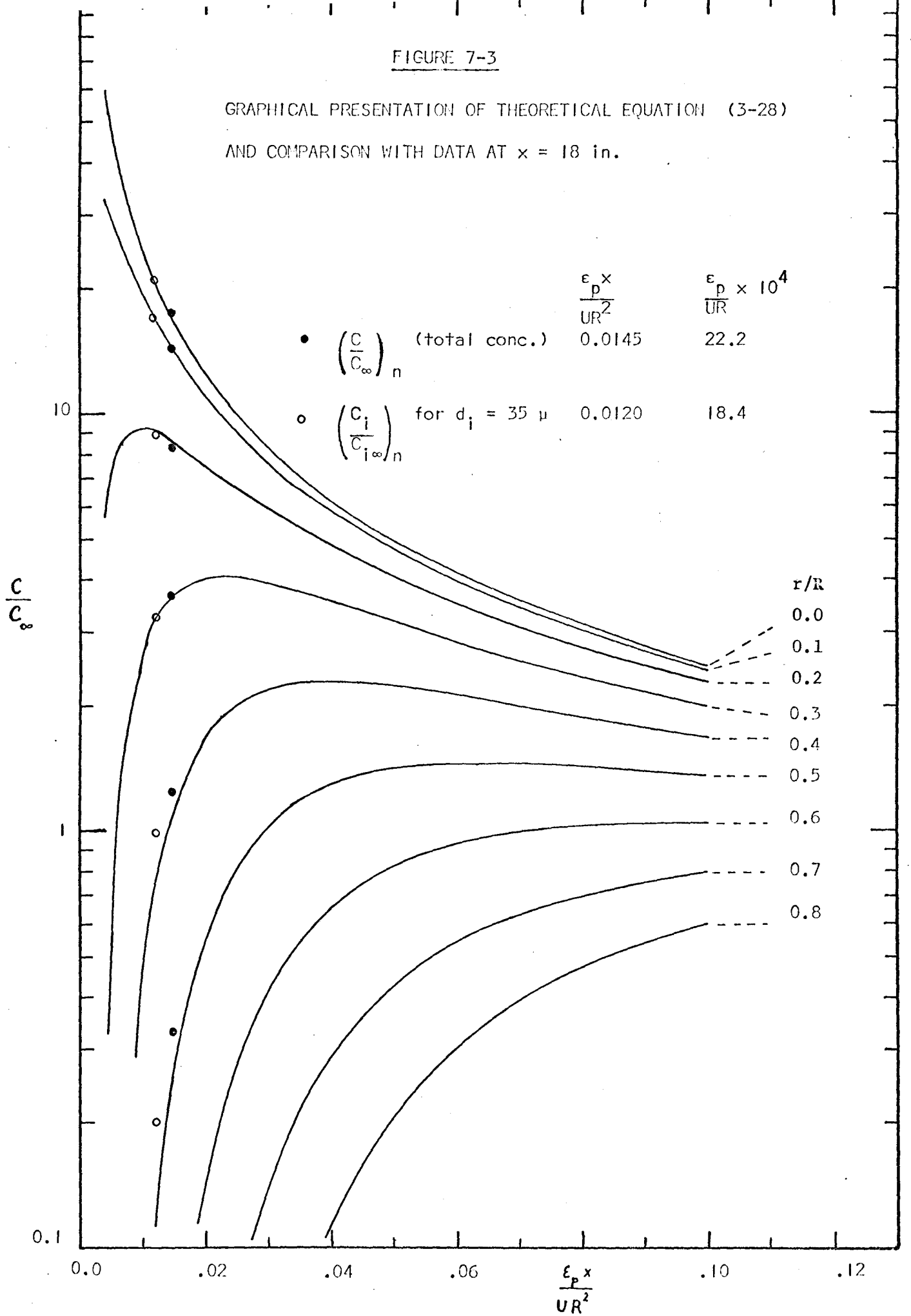

+ 0.6). Therefore the errors due to linear interpolation of profiles C_i/C_∞ were higher in the latter data. In addition, measurements of particle-size distributions were based on 600-800 particles at each sample point of 18 in. profile, whereas only 400 - 600 particles were measured from each of the samples taken further downstream. A larger number of particles, say for example 1000 particles, should be counted for a better statistical representation.

7.2.2. Method 2

(a) Outline of the Method

In many respects,this method follows closely that given in Method I except that the calculation scheme predicts what the radial mass distribution should be at a given axial distance with an assumed eddy diffusivity. The details are given below:

Assuming a value of $\varepsilon_p x/UR^2$, a value of ε_p/UR at any given axial position, x, can be obtained. Figure 7-3 allows a value of C/C_∞ to be found at any radial position r/R. These concentrations are transformed to M_i/M_∞ through equation (7-3a) but now related to each size group in the distribution, i.e.

$$\frac{M_i}{M_\infty} = \left[\frac{C}{C_\infty} f_\infty(d_i)\right]\left(\frac{d_i}{d_{v\infty}}\right)^3 \qquad (7\text{-}17)$$

where $f_\infty(d_i)$, the fraction of particles in size group with average diameter, d_i, in the original feed is given in Figure 4-2.

Each of these size groups are then shifted the appropriate distance

(see Table 7-2) for their size downward to compensate for gravity effects. These profiles are then plotted and at any radial distance, the total mass may be found by addition:

$$\frac{M}{M_\infty} = \sum_i \frac{M_i}{M_\infty} \tag{7-18}$$

This predicted profile is finally to be compared with the experimental data. In practice, several predicted profiles M/M_∞ are drawn for different values of ε_p/UR and from this, the range of ε_p/UR judged to give approximately the best agreement between data and predicted values can be determined.

(b) Numerical Example of Plotting a Predicted Profile

In order to illustrate this method, an example was made to plot a predicted profile at x = 30 in.

Assuming $\varepsilon_p x/UR^2 = 0.025$, then $\varepsilon_p/UR = 22.9 \times 10^{-4}$.

TABLE 7-3

DATA REQUIRED FOR FIGURE 7-4

$\frac{r}{R}$	$\frac{C}{C_\infty}$ at $\frac{\varepsilon_p x}{UR^2} = .025$	Size Group (μ)	d_i (μ)	$f^*_\infty(d_i)$	$\left(\frac{d_i}{d_{v\infty}}\right)^3$	$\frac{\ell}{R}$** at x= 30in.
0.0	10.0	0-10	5	.018	0.003	0.003
0.1	9.0	10-20	15	.107	0.076	0.020
0.2	6.7	20-30	25	.295	0.371	0.066
0.3	4.1	30-40	35	.350	0.968	0.127
0.4	2.0	40-50	45	.185	2.050	0.195
0.5	0.8	50-60	55	.045	3.760	0.270
0.6	0.3					

* values taken from Figure 4-2
* * values taken from Table 7-2

Figure 7-4 presents the profiles M_i/M_∞ after correcting for gravity using data in Table 7-3 and equation (7-17). From Figure 7-4, the total mass profile M/M_∞ was obtained as shown by curve A in Figure 7-6.

(c) Results

The comparison between experimental and predicted mass profiles at four axial positions are presented in Figures 7-5 to 7-8. Typical of predicted profiles as a function of ε_p/UR are also included in Figure 7-5. The results obtained from these figures are summarized in Table 7-4.

TABLE 7-4

VALUES OF PARTICLE DIFFUSIVITY AT 4 AXIAL POSITIONS

x in.	$\frac{\varepsilon_p x}{UR^2}$	$\frac{\varepsilon_p}{UR} \times 10^4$	$\left(\frac{\varepsilon_p}{UR}\right) \times 10^4$ average
18	0.011-0.012	16.9-18.4	17.6
30	0.025-0.027	22.9-24.7	23.8
42	0.034-0.036	22.3-23.6	23.0
54	0.038-0.042	19.0-21.0	20.0

The average value of diffusion coefficient at 4 axial positions is:

$$\frac{\varepsilon_p}{UR} = (21.1 \pm 2.7) \times 10^{-4}$$

or

$$\varepsilon_p = (9.3 \pm 1.2) \times 10^{-3} \text{ ft}^2/\text{sec}$$

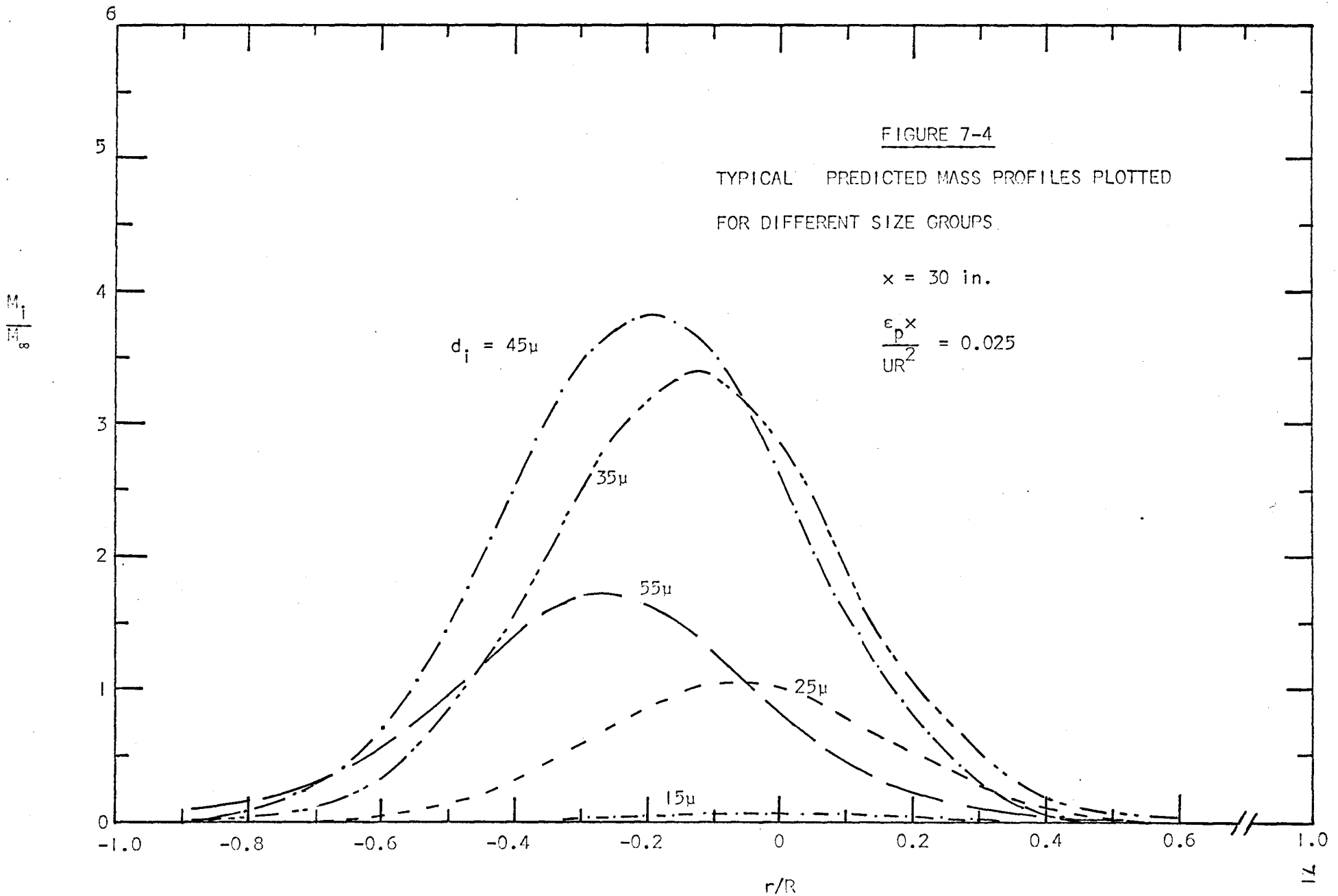
FIGURE 7-4
TYPICAL PREDICTED MASS PROFILES PLOTTED
FOR DIFFERENT SIZE GROUPS
x = 30 in.
$\frac{\epsilon_p x}{UR^2}$ = 0.025
d_i = 45μ
35μ
55μ
25μ
15μ
$\frac{M_i}{M_\infty}$
r/R
6
5
4
3
2
1
0
-1.0
-0.8
-0.6
-0.4
-0.2
0
0.2
0.4
0.6
1.0

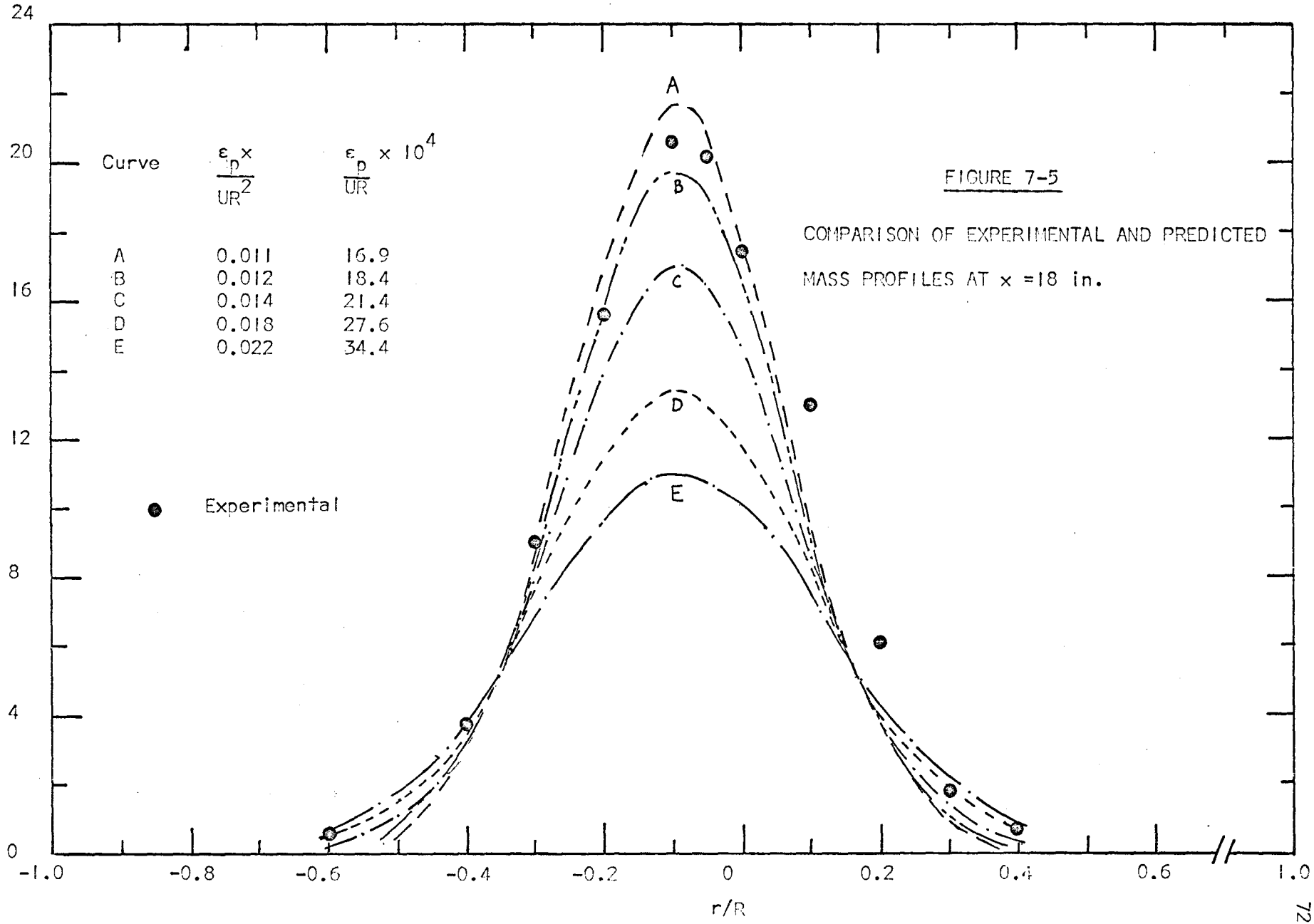

FIGURE 7-5

COMPARISON OF EXPERIMENTAL AND PREDICTED MASS PROFILES AT x =18 in.

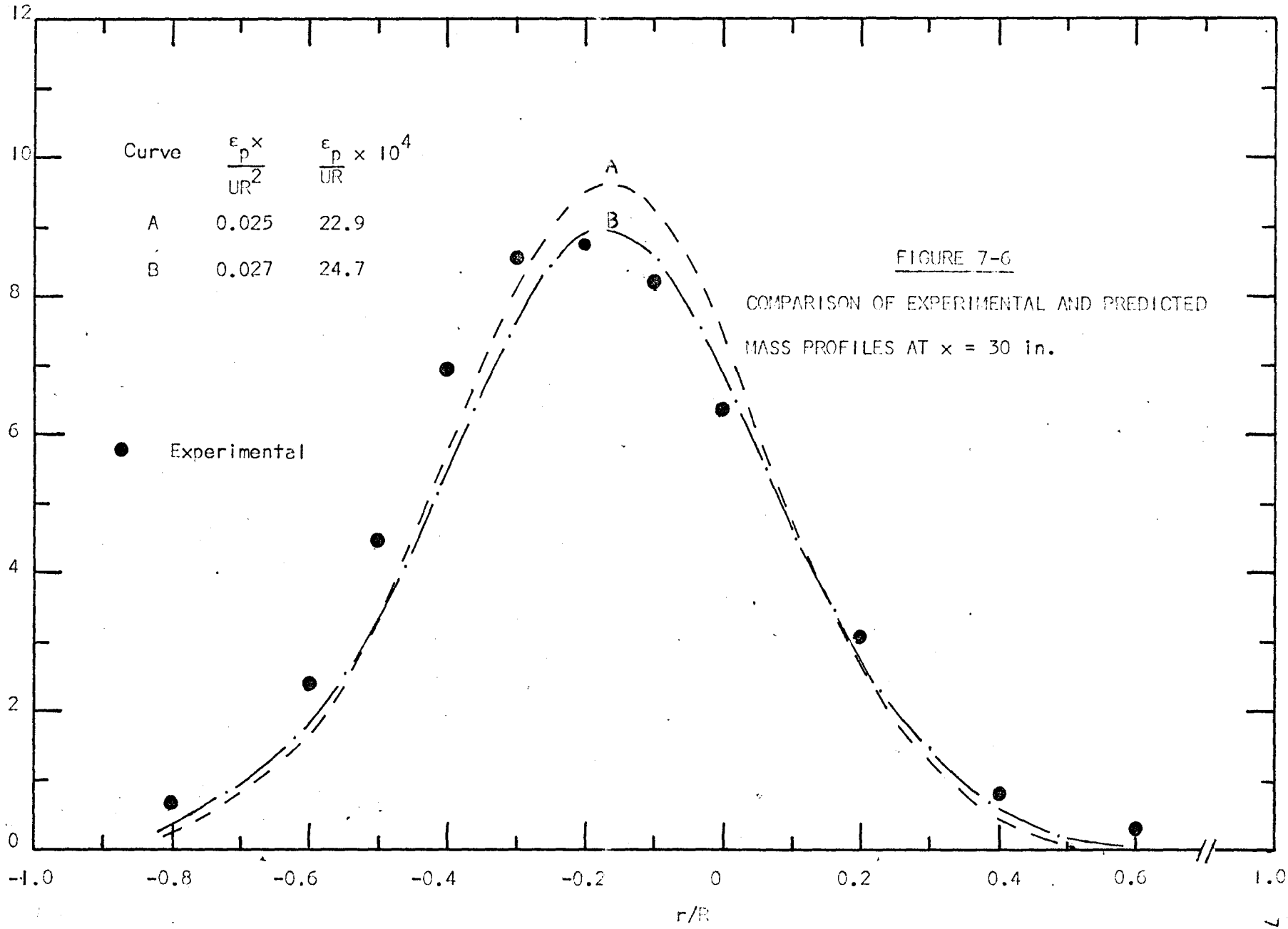

FIGURE 7-6

COMPARISON OF EXPERIMENTAL AND PREDICTED MASS PROFILES AT x = 30 in.

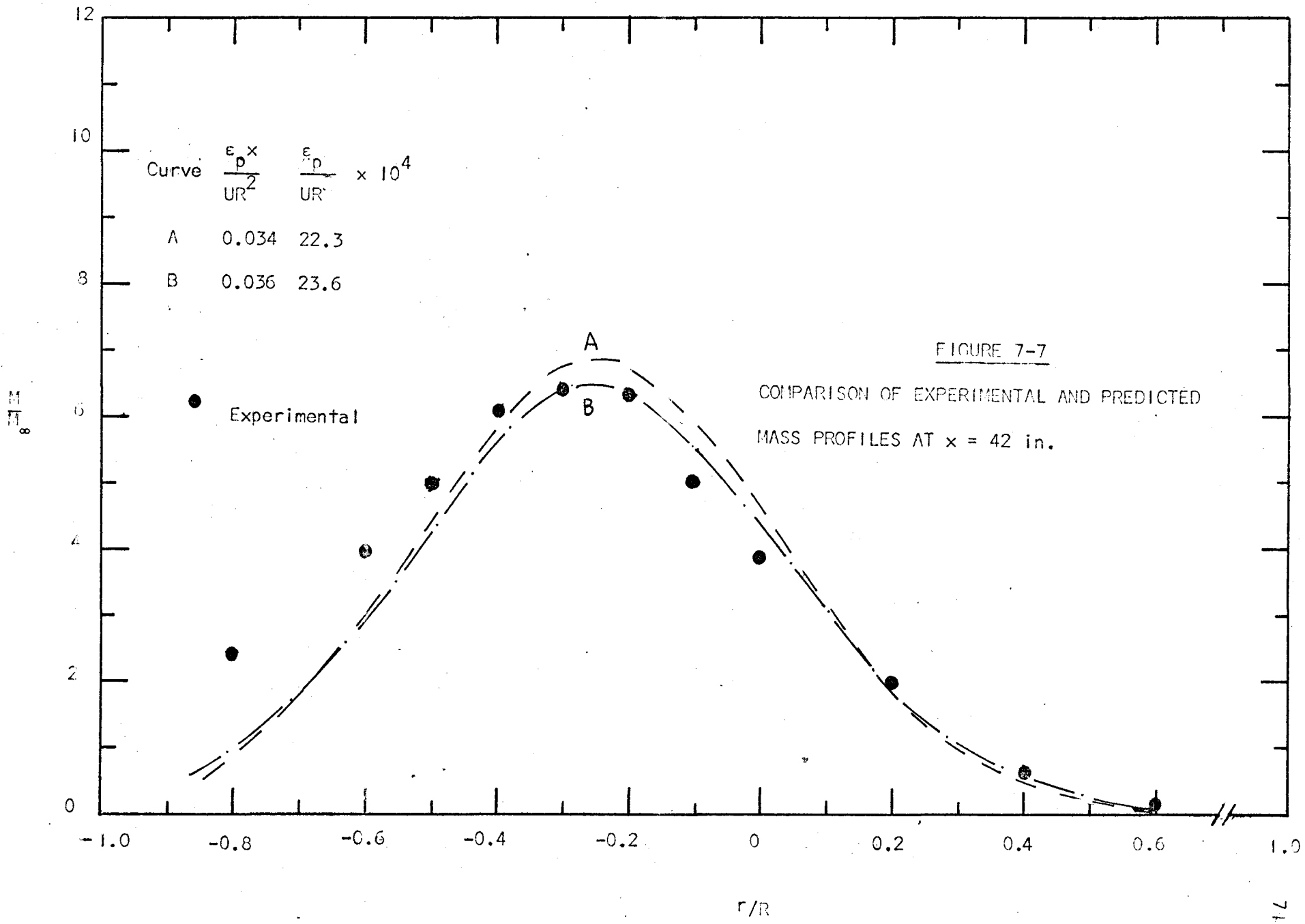

FIGURE 7-7

COMPARISON OF EXPERIMENTAL AND PREDICTED MASS PROFILES AT x = 42 in.

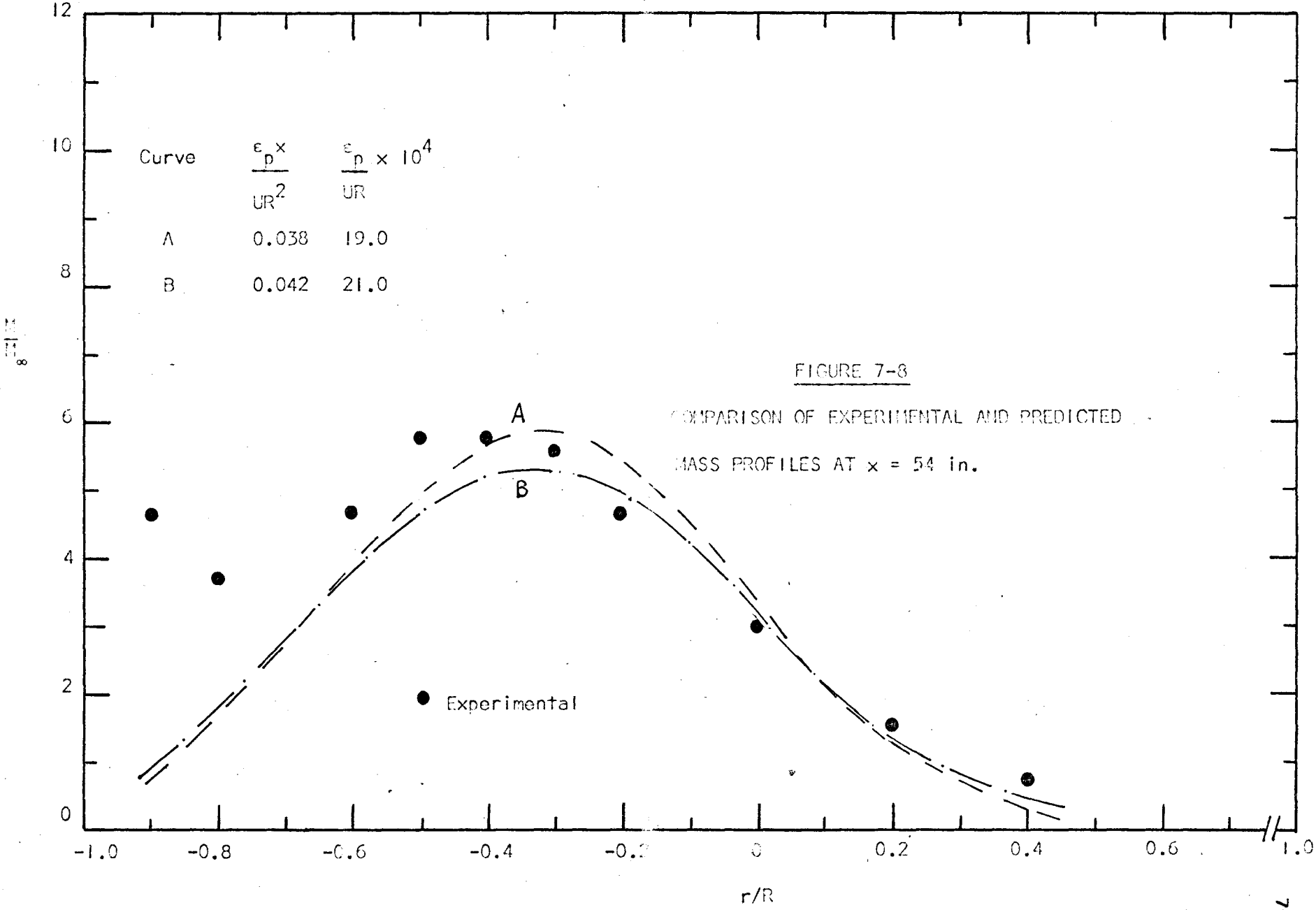

FIGURE 7-8

COMPARISON OF EXPERIMENTAL AND PREDICTED MASS PROFILES AT x = 54 in.

which can be compared with the value of 9.7×10^{-3} ft^2/sec determined by method I for the first profile.

Now it is of interest to estimate the ratio of particle diffusivity to gaseous diffusivity in this turbulent pipe flow, based on the present data and that obtained by Koo for the gas in the same apparatus. Referring to Koo's result in Figure 2-2 (curve 3), the coefficient of gas diffusion at the same Reynolds number of 52800 as that of this work is about:

$$\frac{\varepsilon}{UR} = 35.0 \times 10^{-4}$$

which is compared with

$$\frac{\varepsilon_p}{UR} = 21.1 \times 10^{-4}$$

to give:

$$\frac{\varepsilon_p}{\varepsilon} = 0.60$$

7.3 Calculations Assuming a Functional Relationship Between Particle Size and Eddy Diffusivity.

If the coefficient ε_p changes with particle size, it is of interest to see what effect this might have on the results. One can easily modify the method I to account for this. Instead of adding C_i/C_∞ to get C/C_∞ this method consists of calculating $C_i/C_{i\infty}$ where $C_{i\infty} = C_\infty f_\infty(d_i)$. $C_i/C_{i\infty}$ represents the ratio of the concentration of particles of size d_i in samples over that of the same size in the original tracer when fully mixed with carrier fluid. Other steps described in Section 7.2.1-I remain unchanged.

Unfortunately this technique requires the symmetry of profiles $C_i/C_{i\infty}$ for all sizes. Let us return to the example made for the data at x = 18 in. As can be seen in Figure 7-1, only the profile C_i/C_∞ for d_i = 35 microns is smooth and nearly symmetrical; this suggests that one can

evaluate ε_p for d = 35μ.

The data after dividing C_i/C_∞ by f_∞ (35μ) = 0.35 (Table 7-4) and normalising the profile $C_i/C_{i\infty}$, is compared to equation (3-28) in Figure 7-3. The result is:

$$\frac{\varepsilon_p x}{UR^2} = 0.012$$

or

$$\frac{\varepsilon_p}{RU} = 18.4 \times 10^{-4}$$

The normalising factor in this case was found to be:

$$2\int_0^1 \left(\frac{C_i}{C_{i\infty}}\right) z\,dz = 1.21$$

Because of the experimental techniques adopted in the present study, this method has only a qualitative significance.

8. DISCUSSION

8.1 Evaluation of Experimental Technique

The measurements of profiles of particle mass in the air stream were subject to error from three main sources: the feeding system, the sampling technique and the physical phenomena occuring. Details of these are given below:

8.1.1. Feeding System

Since it took about two hours to obtain a radial profile at any axial position, it was important to maintain constant operating conditions over this period. As pointed out in section 4-2, the solids-feed rate remained constant to within $\pm$ 3% on the average with some rare variations up to $\pm$ 6%, provided the solids level in the lower tank of the feeding system could be kept constant in the range of $\pm$ 0.15 in. by the rotary valve. It was found that the operation of the valve was affected by the humidity of solids. If the solids were too humid, they stuck in the rotor slots; therefore the valve turned but no solids discharged to the lower tank. When the solids were removed and dried, the valve feeder functioned satisfactory.

A second difficulty was that the rotor jammed sometimes during the experiment. This was caused by solid particles entering the ball bearing, although a seal plate was installed to prevent this. When the rotor was disassembled and cleaned, the rotor again turned freely. This factor was not too serious because all runs were short and the valve was cleaned periodically.

Since the solids feed-rate was measured by the weight of solids collected in the cyclone, it was assumed that this device removed all the solids from the gas stream. As the cyclone efficiency was expected to be at least 99%, the loss of solids can be considered negligible in comparison with the variation of the solids feed-rate and other sources of error. Essentially no solids were found in the large chamber in which the cyclone was housed.

Some error in the concentration profile could be attributed to the injector velocity of the solids. Here the injector air velocity was maintained constant to within $\pm$ 2%.

The alignment of the injector is also important. Since great care was taken in installing the injector properly, it was felt that there was small error here.

The conclusion can be drawn that the solids feeder worked satisfactorily during the course of this investigation; variations in solids concentration at any point downstream resulting from the solids feeding system are expected to be less than 5%.

8.1.2. Sampling Technique

The sampling technique depends on the sampling efficiency, i.e. the ability to maintain isokinetic condition at the sampling probe. The isokinetic sampling technique is based on accurately knowing the air velocity at the sampling point. The variations in point velocity are discussed in the following paragraphs:

(a) Turbulent Fluctuations

The air velocity changes with time due to turbulent fluctuations. The intensity of turbulence* is approximately 3% for steady pipe flow; therefore this presents the order of magnitude of the variations in point velocity from this source.

(b) Variations in Fan Speed

The mean velocity was affected by the variation of the motor speed. During the experimental run, the motor speed could be adjusted at 1100 $\pm$ 10 r.p.m.; this corresponded to a velocity at pipe axis of 23.6 $\pm$ 0.2 ft/sec (determined from Figure 6-1). Therefore, the maximum deviation of air velocity was only about 1%.

(c) Variations in Temperature

The room temperature varied from 74°F to 81°F. during the experiment. All data were calculated at the average temperature of 77°F and no correction was made for the runs performed at different temperatures. This temperature variation contributed an error of less than 0.7% on gas properties (density and viscosity), and so can be neglected.

(d) Air Velocity Variations Across the Probe Cross-Section

The sampling probe does not function as a point, but has a finite cross-section. The velocity of the main air stream varies across this cross-section. However, because the probe diameter (0.175 in.) is small compared with the pipe diameter (5.5 in.), this effect is minimized.

---

* The intensity of turbulence is defined as the root-mean square of the instantaneous fluctuating velocity about the mean velocity divided by the mean velocity, i.e., $\sqrt{\overline{u'^2}}/\bar{u}$.

(e) Air Sampling Control

It was found that during the first two minutes of the sampling period, the sampling rate was the most affected by the presence of solids on the filter, but it became nearly constant afterwards. Because of this, the sampling rate required continual attention so that it could be controlled to $\pm$ 5%. Because of other sampling difficulties reported in section 5.2.2., the sampling time at each position, while measuring the solids concentration profile at x = 18 in., was in the range of 2 to 4 minutes, whereas it was from 3 to 7 minutes for other axial positions. Therefore, the error due to the variation of air sampling rate was somewhat higher for the results at x = 18 in. than that downstream.

(f) Probe Position

According to Koo (1), the sampling device could be placed to within a few thousandths of an inch. In this present work, the exact position of the sampling probe was performed by using a magnifying glass on the graduated scale of the traversing mechanism. Therefore, the displacement error again was minimized. This error, if any, might affect the data at x = 18 in. where the particle mass profile is rather sharp, while others are relatively flat.

(g) Misalignment of axis of the probe

The traversing mechanism and the plug at the sampling station hold the probe firmly and the tubing is very sturdy. Thus any deflection caused by the air drag will be very small and the probe should remain pointing directly upstream.

(h) Dimensions of the Probe

The metal wall of the sampling probe was made very thin so that it would not interfere appreciably with the particle movement into the probe.

8.1.3. Special Effects

(a) Gravity Effects

The effects of gravity on experimental results are shown in Figures 6-5 to 6-8. These unsymmetrical profiles could be avoided if the test section was vertical. Also in the figures, we see that the last profile is the most affected by gravity. The high concentration in the region near the pipe bottom may be explained by particles bouncing from the wall and hence increasing the concentrations in this region.

(b) End Effects

At the outlet of the tracer injector, the particle velocity is expected to be somewhat less than the gas velocity. Moreover, the turbulence level of the gas conveying the solids in the injector tube will be quite different from the turbulence in the pipe and hence particle diffusion will be different over the~1/4 in. diameter than in the main pipe flow This will lead to end effects which are very difficult to evaluate.

Both the slip(gas-to-solid)velocity and the end effects vary with position along the duct (20). They will have more significance for the 18 in. profile; at greater distances , they will be a relatively small part of the total process.

All the above considerations may be the reason for which the spread of data points at positions x = 18 in. (Figure 6-5) and x = 54 in. (Figure 6-8)

are relatively higher than that at two middle positions x = 30 in. and x = 42 in. (Figure 6-6 and 6-7). The material balance at each sampling point will be a measure of the error. At x = 18 in., the radial integrated mass of particles (which is inaccurate by virtue of the method of integration as well) is 20% higher than that determined from the weight of solids and flow of gas. Note that this error also includes the inaccuracies in measurement of particle-size distribution. Details of these errors were discussed in section 7.3.1, therefore, they are omitted here.

8.2 Validity of Assumptions

The treatment of data described in Chapter 7, as may be recalled, was based on four main assumptions:

(i) Velocity of particles in axial direction is equal to velocity of gas.

(ii) Drag coefficient of particles is given by Stokes's law: $C_D = 24/Re_p$.

(iii) Velocity and turbulent parameters are constant in the central core.

(iv) Eddy diffusivity is independent of particle size (Methods 1 and 2)

The validity of these assumptions will be discussed in turn.

8.2.1. Particle Velocity

The assumption of equality of fluid and particle velocities seems to be in contrast to our final result on the ratio of particle to fluid diffusivities ($\varepsilon_p/\varepsilon = 0.60$), because if the particles follow exactly the fluid, we should have $\varepsilon_p = \varepsilon$.

At the present time, no established and completely satisfactory procedure is available for treating the motion of particle in a turbulent fluid medium. The general conclusion obtained by many authors, as discussed in Soo's book (25), is that the particle velocity reaches the gas velocity only when the time of contact of gas and particle under steady gas velocity conditions approaches infinity. This slip velocity depends on the particle characteristics (size, density, shape), intensity of turbulence and a fluid (Lagrangian or Eulerian) correlation coefficient, as reported by Friedlander (38) in his study of the behaviour of suspended particles in a turbulent fluid. The author also suggested that for particles larger than 10 μ, this slip velocity becomes important. On the other hand, although Soo (28) obtained experimentally a value of $\varepsilon_p/\varepsilon$ much less than 1, he predicted theoretically that, when the particles are introduced into the duct at nearly zero axial velocity, they accelerate quickly to reach almost the gas velocity in a very short time. For example, Soo's results (28) suggest that for glass particles with diameter 20μ and 50μ, introduced into a gas stream flowing at 20 ft/sec, the duct length required to accelerate the particles to a velocity of 19.9 ft /sec is 3 in. and 16 in. respectively. The above values for gas velocity and particle sizes were chosen because they are of the same order of magnitude with the present data. However, the situation in this study is slightly different. The solids, discharged from the solids feeder into the 1/4 air conveying line, are accelerated by an air velocity approximately 16 times higher than the air velocity at the tracer outlet (1/4 O.D.), because the venturi has a diameter of only 1/16 in. On the other hand, the friction of solids in 1/4 in. tubing may reduce the particle velocity. Therefore, if the two above effects balance

each other, Soo's results indicate that the assumption of equality of fluid and particle velocities in the main pipe flow should not lead to any serious error. It is also expected that the solids flow reaches nearly steady state before it enters the pipe because the effects of the venturi surely are destroyed by the bends and the length (32 in.) of 1/4 in. tubing between venturi and exit.

8.2.2. Drag Coefficient of Particle

The assumption of:

$$C_D = \frac{24}{Re_p} \qquad (7\text{-}6)$$

where Re_p is based on the velocity of particles in direction of fall, is in general, valid for the case of laminar flow with Re_p less than 1. The maximum particle Reynolds number, based on the terminal velocity, for the largest size group (55 microns) in this study, was found to be:

$$Re_p = \frac{dv_t \rho}{\mu} = 0.815$$

Unfortunately, the interaction between the particles and fluid in turbulent flow is far more complex. Torobin and Gauvin (39) have provided a thorough review of the effects of turbulence on the drag coefficient. Both the relative intensity of turbulence and the particle Reynolds number are important factors in determining the drag level. One of the semi-empirical equations referred to by these authors is that of Ingebo (40):

$$C_D = \frac{27}{Re_p^{0.84}} \qquad (8\text{-}1)$$

for the system consisting of a cloud of particles injected from rest into

a moving gas stream. The above expression was obtained from experimental data for Re_p ranging from 6 to 500. If one assumes that equation (8-1) can be extrapolated in the regime of $Re_p<1$, then it will give a drag coefficient slightly higher than that predicted by equation (7-6).

Torobin and Gauvin also pointed out that even in the Stokes law region, the drag force will depend on the previous history of the particle motion. However, this effect is small compared to the large effects noted experimentally for higher Re_p.

8.2.3. Velocity and Turbulent Parameters

Using the assumption of equality of particle and fluid velocities, and assuming a linear trajectory of particle from injector mouth to any position (r,x) downstream, it was found by a simple finite difference technique that the average particle velocity in flow direction is constant within $\pm$ 2.5% up to radial position $r/R = \pm 0.6$. Therefore, in this region, the assumption $u_p = u_c$ (gas velocity at pipe axis,) does not introduce any serious error in the correction for gravity.

As indicated earlier in this report, the turbulent gas diffusivity was expected to be fairly constant over the central core. If this is the case then the fact that the concentration of particles is asymmetric

(relative to the pipe axis) is not important; thus, the cylindrical coordinates can be assumed to be moving downward with the particles, as assumed.

However, referring to Koo's results (Figure 2-1), we find that the the eddy diffusivity in the pipe is less constant than the eddy viscosity obtained by Reichardt (8) and by others presented in reference (20). Koo also reported that his calculations on $\varepsilon(r)$ were subject to many errors which exist particularly in the region near the wall and at the pipe axis. Therefore, the exact profile of gas diffusivity is not known with accuracy because of the lack of experimental data.

8.2.4. Diffusivity versus Particle Size

No effect of particle size was noted, but the sensitivity of the present experimental technique does not give a clear indication of this. As shown in Figure 7-4, the contribution to the sample mass of particles of size less than 25μ is negligible compared with the larger sizes.

In the past, there was little information concerning the variation of diffusivity with particle size. The works of Kalinske and Pien (32) and Rouse (31) on the study of combined diffusion and setting of suspended particles in water indicated that this variation is small.

8.3 Discussion of Results

The experimental errors as well as the assumptions considered above are the reasons for the deviation between the experimental and predicted mass profiles shown in Figures 7-4 to 7-7.

The weakness of method 2, in this analysis, is that one cannot normalize the experimental results in order to eliminate all experimental

errors, in contrast with method 1.

As only the data at x = 18 in. is reliable for both methods, the difference between two results can only be discussed on the basis of this one observation. Method 1 gives $\varepsilon_p/UR = 22.2 \times 10^{-4}$, whereas method 2 gives a value of 17.6×10^{-4}. The difference between two values is 24%. It should be remembered that the data in method 1 was normalized by a factor of 1.20. Assuming that this error (20%) is due mainly on the original data M/M_∞, then if the latter is corrected by the same factor (1.20), the data, once normalized, should fall onto the curve C (Figure 7-5) which corresponds to $\varepsilon_p/UR = 21.4 \times 10^{-4}$. In this case, the difference between two results reduces to only 4%. However, the normalizing factor is, in general, not known in method 2; therefore, in order to present the true picture of experimental errors, no correction was made for all data in method 2.

It should be noted that the deviation between experimental and calculated profiles is less at x = 30 in. and x = 42 in. This suggests that the experimental data may be more accurate at greater distances from the injector.

For the data at x = 54 in. (Figure 7-8), the deviation between experimental and calculated points in the regions of the wall is due mainly to the gravity effects discussed previously. In these regions as well, the assumptions are less applicable.

Although the experimental errors are difficult to estimate and the assumptions discussed previously are open to question, the little variation of ε_p/UR determined at various axial positions by two methods

indicates that the value of ε_p may be reasonably accurate. This gives one confidence that the values determined in an experiment in a vertical flow might be essentially the same. For this reason, it is of interest to compare the results of this work with those of other workers; these are shown in Table 8-I. In spite of the wide difference of gas-solids flow conditions in these various investigations, Table 8-I indicates that the particle diffusivity for glass beads found here is of the same order of magnitude as that found by Soo (35) and by Van Zoonen (30).

The particle-to-gas diffusivity ratio found in this experiment was 0.60. Rouhiainen and Stachiewicz (27) predicted theoretically a value of $\varepsilon_p/\varepsilon = 0.36$ for lycopodium particles ($d_p = 32\mu$, $\rho_p = 0.62$ g/cc) at the same Reynolds number (Re = 52800) as that in this work. Their model would predict a lower ratio for higher density glass particles ($\rho_p = 2.55$ g/cc). Their model had many questionable assumptions in it, however.

TABLE 8-1

COMPARISON OF PRESENT RESULTS FOR PARTICLE DIFFUSIVITY WITH THOSE OF OTHER WORKERS

Reference	Pipe dia. (in)	u_c (ft/sec)	Particle	d (μ)	$\frac{W_p}{W}$	$\varepsilon_p \times 10^3$ (ft^2/sec)
Soo(35)	5.0	132.2	Glass	50	4.97	8.56
"	"	128.4	"	"	8.13	11.10
"	"	138.3	Magnesia	35	0.25	1.24
"	"	137.6	"	"	0.55	1.71
"	"	136.9	"	"	0.88	2.05
Soo(34)	3.0	100.0	Glass	100-250	0.08	2.90
Van Zoonen(30)	2.0	27.8	Catalyst*	20-150	23.7	8.60
"	"	29.7	"	"	55.7	10.15
"	"	31.1	"	"	106.5	14.0
Present Study	5.5	23.6	Glass	0-60	~0.01	9.76(1)** 9.30(2)

* The type of Catalyst is not available

** Methods 1 and 2 respectively

9. CONCLUSIONS AND RECOMMENDATIONS

The following conclusions were drawn from this study:

(a) For the particles and system employed, the particle diffusion coefficient was found to be 9.30×10^{-3} ft^2/sec; this is 40 percent less than the corresponding gas diffusion coefficient.

(b) The effects of gravity on glass particles were found to overly complicate the analysis for turbulent diffusion in a horizontal test section. Because of the uncertainties introduced in accounting for this effect, some error in the diffusivity may be introduced.

(c) The non-uniformity of particle sizes also made the experimental work and analysis extremely difficult. Moreover, the effect of particle size has not been ascertained.

Therefore, the following recommendations are made to guide any future work.

(a) The pipe should be installed vertically.

(b) The particles should be of uniform size.

(c) The dependence of the particle-diffusion coefficient on particle density and size, and flow Reynolds number should be determined experimentally.

10. REFERENCES

1. Koo, J.K., M. Eng. Thesis, Mechanical Engineering Department, McMaster University, (1967).

2. Koo, J.K. and Wade, J.H.T., C.A.S.I. Transactions, 2, 58 (1969).

3. Hinze, J.O., "Turbulence - An Introduction to its Mechanism and Theory", McGraw-Hill, New York (1959).

4. Wasan, D.T. and Wilde, C.R., Int. J. Heat and Mass Transfer, 7, 87 (1964).

5. Von Karman, J., Trans. A.S.M.E., 61,705 (1939).

6. Gill, W.N. and Scher, M., A.I.Ch.E. Journal, 7, 61 (1961).

7. Lin, C.S., Moulton, R.M., and Putnam, G.L. Ind. Eng. Chem., 45, 636 (1953).

8. Reichardt, H., Z Angnew. Math. Mech. Bd., 31 N. 7 (1951).

9. Deissler, R.G., N.A.C.A. Report 1210 (1955).

10. Towle, W.L., and Sherwood, T.K., Ind. Eng. Chem., 11, 457 (1939).

11. Wilson, H.A., Proc. Cambridge Phil Soc., 12,406 (1904).

12. Sherwood, T.K., and Woertz, B.B., Trans. Am. Inst. Chem. Engrs., 35, 517 (1939).

13. McCarter, R.J., Stutzman, L.F. and Koch, H.A. Jr., Ind. Eng. Chem., 41 1290 (1940).

14. Flint, D.L., Kada, H. and Hanratty, T.J., A.I.Ch.E. Journal, 6, 624 (1960).

15. Klinkenberg, A., Krajenbrink, H.J., and Lauwerier, H.A., Ind. Eng. Chem., 45, 1202. (1953).

16. Shlinger, W.G., and Sage, B.H., Ibid, 45,627 (1953).

17. Taylor G.I., Proc. Roy. Soc., A151, 421 (1935).

18. Ibid., A223, 446 (1754)

19. Baldwin, L.V., and Mickelson, W.R., J. Eng. Mech. Div. Am. Soc. Civ. Engrs., 88, 42 (1963).

20. Boothroyd, R.G., Transt. Inst. Chem. Engrs., 45, T297 (1967).

21. JohnK, R.E., and Hanratty, T.J., Technical Report No.10, University of Illinois, February 1961.

22. Alexander, L.G. and Coldren, C.L., Ind. Eng. Chem., 43, 1325 (1951).

23. Kesler , G.H., Sc. D thesis, Massachusetts Institute of Technology (1952).

24. Soo S.L., Chem. Eng. Sci., 5,57 (1956).

25. Soo, S.L., "Fluid Dynamics of Multiphase Systems", Blaisdell Publishing Co. (1967).

26. Peskin, R.L., Proc. of the 1960 Heat Transfer and Fluid Mechanics Institute, Stanford University Press, Stanford, California. (1960).

27. Rouhiainen, P.O., and Stachiewicz, J.W., A.S.M.E., 69 HT-41 (1969).

28. Soo, S.L., Ihrig, Jr. H., and Elkouh, A.F., Journal of Basic Eng., 609 (1960).

29. Farmer, R.C., Ph.D thesis, Georgia Institute of Technology (1962).

30. Van Zoonen, D., "The Interaction Between Fluids and Particles", London: The Institute of Chemical Engineers, p. 64 (1962).

31. Rouse, H., "Proceedings of the Fifth International Congress of Applied Mechanics", p.550, John Wiley and Sons, New York (1939).

32. Kalinse, A.A. and Pien, C.L., Trans. Am. Geophys. Union, 24, Part II, 530 (1943).

33. Longwell, J.P., and Weiss, M.A., Ind. Eng. Chem., 45, 667 (1953).

34. Soo S.L., Ind. Eng. Chem. Fund., 1, 33 (1962).

35. Soo S.L. et al., Ibid., 3, 98 (1964).

36. Jenson, V.G., and Jeffreys,G.V. "Mathematical Method in Chemical Engineering", Academic Press Inc., London (1963).

37. Julian, F.M., and Du kler, A.E., A.I.Ch.E. Journal, 11, 853 (1965).

38. Friedlander, S.K., Ibid., 3, 381 (1957).

39. Torobin, L.B. and Gauvin, W.H., Can. J. Chem. Eng., (37), 129-41, 167-176, 224-236 (1959); 38, 142-153, 189-200 (1960); 39, 113-120 (1961).

40. Ingebo, R.D., N.A.C.A., TN3762 (1956).

41. Sherman, F.S., N.A.C.A. TN 2995 (1953).

42. Chistova, E.A., "Tables of Bessel Functions of the True Argument and of Integrals Derived from Them," Pergamon Press, London (1959).

APPENDIX

A.1 Gas Velocity Calculations

The familiar equation for the evaluation of velocity using the Pitot tube is:

$$u = C_o \sqrt{2g_c \Delta H} \qquad \text{(A-1)}$$

where ΔH is expressed as a head of air.

Under the condition of this experiment, the Reynolds number based on the diameter of the Pitot tube and the air velocity measured was always greater than 500; therefore the coefficient C_o is unity (4 1).

The average velocity U was obtained by integrating the velocity profile (Figure 6-3) across the flow section:

$$U = \frac{1}{\pi R^2} \int_0^R 2\pi r u dr \qquad \text{(A-2a)}$$

or

$$U = 2 \int_0^1 u \, z dz \qquad \text{(A-2b)}$$

The numerical value of U was found to be 19.2 ft/sec.

The flow Reynolds number is:

$$Re = \frac{2RU\rho}{\mu} \qquad \text{(A-3)}$$

with 2R = 5.5 in.

$$\rho = 0.0744 \text{ lbm/ft}^3$$

and $\mu = 0.0183$ c.p. $= 0.123 \times 10^{-4} \frac{\text{lbm}}{\text{ft-sec}}$

for air at average temperature of $77^{o}F$, the value of Re is:

$$Re = 52800$$

The volumetric flow-rate:

$$Q = \pi R^2 U = 191 \text{ ft}^3/\text{min}$$

The mass flow-rate:

$$W = Q\rho = 13.37 \text{ lb/min.}$$

The dimensionless velocity profile was calculated from the symmetrical profile by using the following expressions:

$$u^* = \sqrt{f/8}\, U \qquad (A-4)$$

$$u^+ = u/u^* \qquad (A-5)$$

$$y^+ = y\frac{u^*}{u} \qquad (A-6)$$

where u^* is the friction velocity $\left(\sqrt{\frac{\tau_w g_c}{\rho}}\right)$ and y is the distance from wall = R - r.

An example follows:

$$u = 21.3 \text{ ft/sec at } r/R = 0.6 \text{ (Figure 6-3)}$$

$$y = R-r = \frac{2.75}{12} - 0.6 \times \frac{2.75}{12} = 0.0916 \text{ft.}$$

From the Moody diagram, the friction factor f for smooth pipe at Re = 52800 is 0.205. Hence:

$$u^* = \sqrt{\frac{0.205}{8}} \times 19.2 = 0.98 \text{ ft/sec}$$

$$u^+ = 21.3/0.98 = 21.7$$

$$\nu = \frac{\rho}{\mu} = \frac{0.0744}{0.123 \times 10^{-4}} = 0.1665 \times 10^{-3} \text{ ft}^2/\text{sec}$$

$$y^+ = (0.0916)\ \frac{0.98}{0.1665 \times 10^{-3}} = 542$$

This is the data shown in Figure 6-4.

A.2 Numerical Solutions of Theoretical Equation (3-28)

Equation (3-28) was solved on an I.B.M. 7040 digital computer. The university library subroutine BESSJ was used to calculate the Bessel functions J_o and J_1. The values of β_n, roots of $J_1(\beta_n) = 0$, were taken from tables of Bessel functions (42). It was found that the values of C/C_∞ for n = 14 and n = 31 are the same up to 5 significant figures, i.e., the series in equation (3-28) converges rapidly to a constant. Therefore, only the first 14 values of β_n were included in the computer program. Details of this are given below:

```
C  COMPUTER PROGRAM TO CALCULATE THE THEORETICAL CONCENTRATION
C  IN FUNCTION OF RADIAL POSITION AND DIMENSIONLESS GROUP DIFF
C
C  RC= C/C∞
C  DIFF= ε*X/(U*R**2)
C  Z=r/R
C  BETA= ROOTS OF J1 (BETA)=0
C  R= PIPE RADIUS (2.75 IN.)
C  B= TRACER INJECTOR RADIUS (0.117 IN.)
C
C  Z VARIES FROM 0.0 TO 0.8 BY 0.1 INCREMENT
C  DIFF VARIES FROM 0.005 TO 0.1 BY 0.005 INCREMENT
C
      DIMENSION BETA(14),WORK(100)
      DATA R,B/ 2.75, 0.117/
      READ(5,2) (BETA(I), I=1,14)
      Z=0.00002
      DO 40 L=1,9
      DIFF= 0.005
      DO 50 LL=1,20
      SUM=0.0
      DO 100 I=1,14
      A= BETA(I)*B/R
      C= BETA(I)*Z
      E= BETA(I)
      D= -BETA(I)*BETA(I)*DIFF
      Y1= BESSJ(A,1.0,WORK)
      Y2= BESSJ(C,0.,WORK)
      Y3= BESSJ(E,0.,WORK)
      Y4= Y1*Y2*EXP(D)
      Y5= BETA(I)*Y3*Y3
  100 SUM=SUM+ Y4/Y5
      RC =1.0 + 2.0*R*SUM/B
      WRITE(6,81)  Z,DIFF,RC
      DIFF= DIFF + 0.005
   50 CONTINUE
      Z=Z+0.1
   40 CONTINUE
    2 FORMAT(7F10.0)
   81 FORMAT(// 10X, 2HZ=, F5.2, 5X ,5HDIFF=,F10.3, 5X, 3HRC=, F10.4/)
      STOP
      END
```

A.3. Calculations of ℓ/R for Gravity Correction

From equation (7-14):

$$\frac{\ell}{R} = \frac{v_t}{R}\left(\frac{x}{u_c}\right) - \frac{v_t}{Rk}\left[1 - \exp\left(-k\frac{x}{u_c}\right)\right] \qquad (7\text{-}14)$$

where

$$k = \frac{18\mu}{d^2\rho_p} \qquad (7\text{-}10a)$$

$$v_t = \frac{g(\rho_p - \rho)\, d^2}{18\mu} \qquad (7\text{-}10b)$$

(a) $$k = \frac{18 \times 0.0183 \times 10^{-2} \ \frac{gm}{cm\text{-}sec}}{d^2 \times 10^{-8} \ cm^2 \times 2.55 \ \frac{gm}{cm^3}}$$

$$k = \frac{129}{d^2} \times 10^3 \ sec^{-1}$$

in which d is in microns.

(b) Since the gas density is negligible in comparison with solids density, the terminal velocity becomes:

$$v_t = \frac{gd^2\rho_p}{18\mu} = \frac{g}{k}$$

$$= \frac{32.2 \ \frac{ft}{sec^2} \times 12 \ \frac{in}{ft}}{\frac{129}{d^2} \times 10^3 \ sec^{-1}}$$

$$= 2.99 \times 10^{-3} \ d^2 \ in/sec$$

(c) The values of k and v_t, once introduced into equation (7-14) will give ℓ/R as a function of d (microns) and x (in.).

A sample calculation follows: for d = 35μ and x = 18 in., we have:

$$\frac{v_t}{R}\left(\frac{x}{u_c}\right) = 0.083 \quad (\text{Note } u_c = 23.6 \text{ ft/sec})$$

$$\frac{v_t}{Rk} = 0.0126$$

$$1 - \exp\left(-\frac{kx}{u_c}\right) = 0.9987$$

Hence

$$\frac{\ell}{R} = 0.083 - 0.0126 \times 0.9987$$

$$= 0.070$$

Table 7-2 showed the complete results for ℓ/R at four axial positions for 6 size groups.